A MODEL FOR THE STUDY OF FAST TRANSIENTS ON A D-C DISTRIBUTION SYSTEM

GEORGE S. HAMILTON
and
URBAN R. LAMAY

A MODEL FOR THE STUDY OF FAST TRANSIENTS ON A D-C DISTRIBUTION SYSTEM

* * * * *

George S. Hamilton

and

Urban R. Lamay, Jr.

A MODEL FOR THE STUDY

OF

FAST TRANSIENTS ON A

D-C DISTRIBUTION SYSTEM

by

George S. Hamilton

Captain, United States Marine Corps

and

Urban R. Lamay, Jr.

Lieutenant, United States Navy

Submitted in partial fulfillment of
the requirements for the degree of

MASTER OF SCIENCE
IN
ENGINEERING ELECTRONICS
AND
ELECTRICAL ENGINEERING

respectively

United States Naval Postgraduate School
Monterey, California

1 9 6 5

A MODEL FOR THE STUDY OF FAST TRANSIENTS ON A D-C DISTRIBUTION SYSTEM

by

George S. Hamilton
Captain, United States Marine Corps

and

Urban R. Lamay, Jr.
Lieutenant, United States Navy

This work is accepted as fulfilling

the thesis requirements for the degree of

MASTER OF SCIENCE

IN

ENGINEERING ELECTRONICS
AND
ELECTRICAL ENGINEERING

respectively

from the

United States Naval Postgraduate School

ABSTRACT

Fast voltage transients have been found capable of disrupting the operation of a proposed solid-state, ac-dc inverter system. A method is proposed for studying the propagation of such transients in an involved d-c power distribution system connected to such an inverter. The use of computer simulation of the system is proposed and detailed. Mathematical equivalents of various circuit elements are developed, and signal flow graphs are used to write the system's equations in a form adapted to the computer. Use of this method is shown to allow a large number of system locations to be chosen as inputs or as points of measurement, even when the simulation is programmed for a digital computer.

ACKNOWLEDGEMENTS

The authors wish to express their appreciation to Doctor James S. Demetry for his guidance and encouragement throughout this study, and to the Bureau of Ships and the General Electric Company who generously provided necessary source material.

TABLE OF CONTENTS

LIST OF ILLUSTRATIONS

1. Introduction.

1.1 The Bureau of Ships, alert to the potential of static power conversion equipments for use between d-c and a-c power distribution systems, has conducted studies and has contracted for studies of the feasibility of shipboard installation of such equipments. The advantages of static power conversion devices over motor-generators are numerous. "The static inverter, being solid state throughout, has no moving parts, needs no lubrication, is lighter, uses less floor space and has greater efficiency than its rotating counterpart." [5] The studies initiated by the Bureau of Ships have included the factors of cost, reliability, maintainability, space, weight, and environmental considerations, as well as a-c and d-c systems performance.

1.2 The purpose of this paper is to plan in detail the study of one of the problems that has been found in pilot systems where such equipments have been installed. That problem is the presence of fast, high voltage transients at the d-c input terminals of the inverter caused by faults and fault clearances.

1.3 Although the study described herein is concerned primarily with the d-c distribution system and only remotely with the conversion equipment, a brief description of the sensitive solid-state device is necessary to the understanding of why the voltage transients are of concern. The principle load-carrying element of the solid-state, static inverter is the silicon-controlled rectifier, SCR, a four layer device which utilizes three p-n junctions and three terminals to perform its functions: reverse-bias blocking; forward-bias blocking; and controlled switching to the conduction state from the forward blocking state. High voltage transients

across the SCR, when they exceed the peak inverse voltage of the device, can appreciably shorten its life, and if sufficiently severe, can cause its immediate failure. E. K. Howell, of the General Electric Corporation, describes an additional limitation of the SCR when subjected to fast transients, "...false triggering by the dV/dt effect. When in the blocking forward-biased condition, the center junction of the SCR is essentially a capacitor connected between the anode and the gate. If the anode voltage is changed, a displacement current will flow through this capacitor equal in value to the product of the capacitance and the rate of change of anode voltage, dV/dt. A high dV/dt caused by a fast transient can trigger the SCR into conduction" [2] . Such spurious gating of an SCR at the d-c side of an inverter may result in one or more of the following effects at the a-c output:

Frequency drift

Voltage variation

Harmonic distortion of the a-c voltage waveform.

1.4 Specifically, the problem was to determine the magnitude and rate of rise of voltage produced at the inverter by sudden interruption or initiation of large currents elsewhere in the d-c system and to determine what the effects would be if the system were slightly modified. System simulation with a computer was the method of analysis chosen. The bulk of the study is adaptable to either a digital or analog computer. Only in the final stages, section 5.1.2., is a commitment made in order to solve the particular problems of this particular system. The advantages and disadvantages of the chosen course, digital computer simulation, are discussed and details of a suitable program (Fortran '60) are outlined.

2. D-C Distribution System.

2.1 General Description

A block diagram of the d-c system showing major components and interconnecting cable is presented in Fig. 2-1. The basis for this diagram are references [3] and [4] . Not all loads indicated in those references are included in Fig. 1, nor are they considered in any of the subsequent development. Their omission is justified by the following considerations:

a. The emphasis of this investigation is upon developing techniques and procedures for studying fast transients. Given the distribution system of a particular class of submarines, and using the suggested circuit models and simulation procedures, the response of the system to a steep wavefront current can be readily predicted. The validity of the techniques is not dependent upon the number of loads chosen for this development, but rather upon the accuracy of the component circuit models, and upon the assumption that all significant d-c loads and transmission components can be represented by the proposed models;

b. Omitted loads are in such a location that they would not affect the transients at the chosen points of interest were they included;

c. Circuit protection equipment (fuses, circuit breakers, low voltage relays, etc.) are omitted. The transients of concern are very fast compared to the reaction time of these devices; that is, the transient will have reached peak magnitude before the protective equipment can operate to interrupt the transmission in any branch.

d. The detailed plans for those submarines for which this study may be of interest are classified.

From the block diagram it can be seen that there are two distribution system, port and starboard, tied together electrically at the battery.

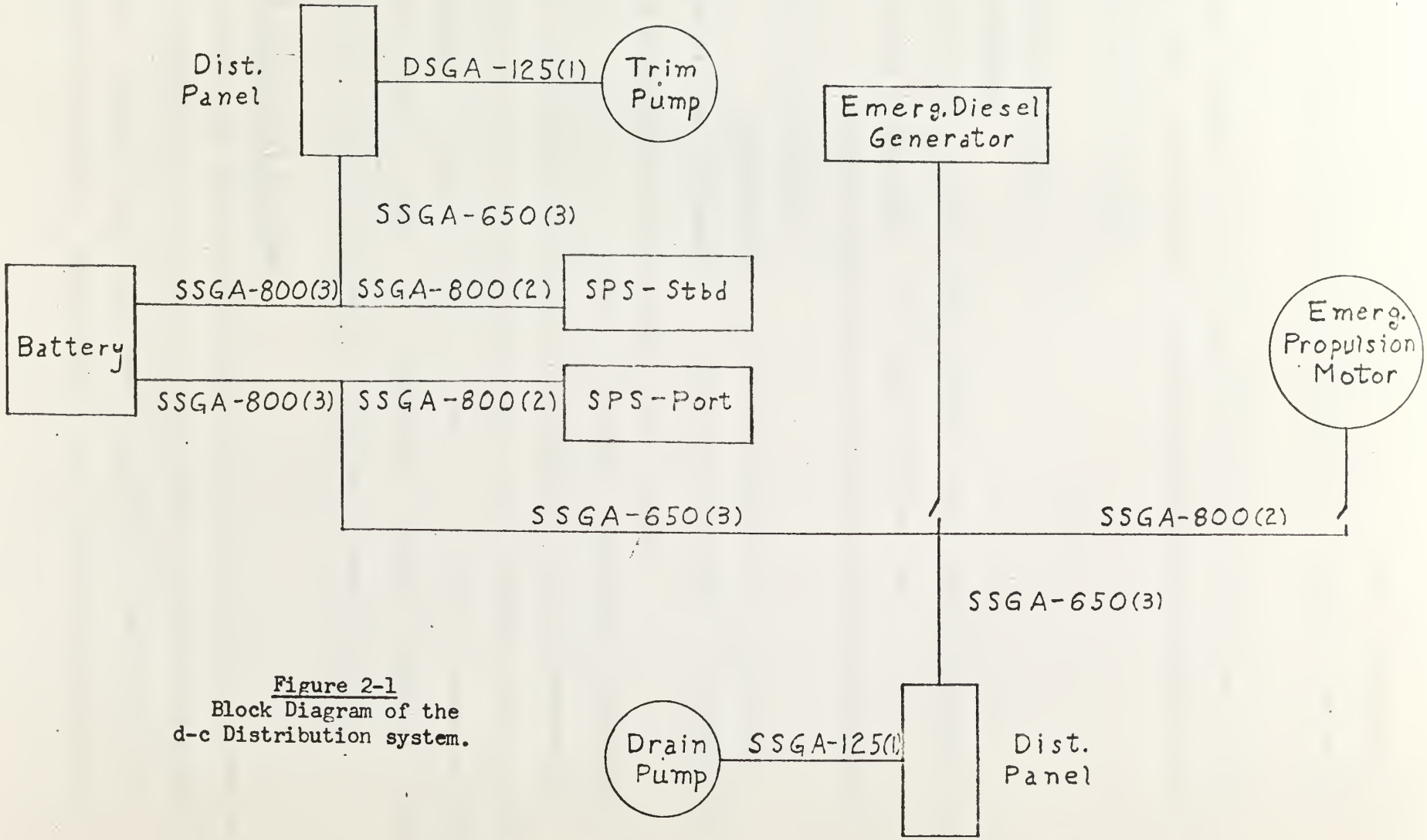

Figure 2-1
Block Diagram of the
d-c Distribution system.

With battery breakers open, each system can be operated independently with power supplied by the a-c to d-c conversion equipment (see section 2.2.4).

As is standard for all shipboard electrical installations, the d-c system floats with respect to the ship's structure, and thus comprises a complete electric circuit.

2.2 System Components

2.2.1 Battery

The battery provides a high capacity energy source with nominal output voltage of 250 volts. Its primary functions are:

a. Provide power for all control and instrumentation circuits during reactor startup;

b. Provide power to essential circuits, a-c and d-c, when reactor has been "scrammed" or is otherwise shut down, or is functioning at too low a power level to operate these circuits.

The linear circuit model of the battery is developed in Appendix C. Note: Considerable use is made of the Laplace transform wherever the occurrence of linear relationships among circuit variables render its use advantageous. Its use, however, is nowhere essential; it can be replaced completely with analysis in the time domain. The use of upper-case letters for system variables indicates the transform of those variables.

2.2.2 Trim and Drain Pumps.

These pumps, one fed by the port bus, the other by the starboard bus, are representative of any of the d-c motor loads. They are the largest motors, in terms of both horse power and mechanical inertia, that are frequently on the line. Their linear circuit model is also developed in

2.2.3 Emergency Propulsion Motor Feeder.

This feeder is included to show the effects of any load feeder which is open-circuited at the load end. The circuit model for this feeder is identical to that of all the other transmission cable discussed in 2.2.5.

2.2.4 Static Power Supply (SPS).

On nuclear powered submarines currently in commission, power conversion between the a-c and d-c systems is effected through motor-generators. There are usually two such machines, each rated at 300KW, and each capable of two-way operation. In this study each motor-generator is considered replaced by its static equivalent, the SPS. It is the solid state devices which comprise the load-carrying circuits of the SPS that are sensitive to the fast transients. The passive circuit model of the SPS depends upon which of several possible circuits is used. In Appendix C, one such circuit has been shown, and the branch termination representing the input impedance of the SPS has been established from this circuit, based upon the selected mode of operation.

2.2.5 D-C Bus and Load Feeders.

The d-c buses, port and starboard, consist of single-conductor, shielded, copper cables (SSGA), the number and size of which in any part of the system depend upon the rated load of that part. Between the distribution panels and individual loads, two-conductor, shielded cables (DSGA) are used. In Fig. 2-1 the cable type designation is followed by the nominal size of the cable (expressed in thousands of circular mils); the number of cable pairs is shown in parenthesis following the size.

The transients of concern are short duration, high frequency voltage components superimposed upon the normal d-c line voltage, or upon slower transients. This means that cables must be considered as transmission lines. In Appendix B, expressions for the distributed parameters of the cables are developed, and in Section 3, a lumped parameter equivalent model is established.

3. Modeling the Connecting Cables as Transmission Lines

3.1 Transmission Line Simulation.

The sets of cables were reduced to a single transmission line by replacing the distributed parameters of the individual cables with equivalent distributed values, and by saying that all losses and interactions occur only in one conductor of the pair. On this conductor, all voltages were measured above a ground which is designated as the electrical midpoint of the real, balanced circuit.

The duration of the transients considered was in the range of one to fifty microseconds [6] . Since this is the same order of magnitude as the time required for a wave front to propogate the length of the cables, the propogation time must be taken into account in the model and the cables must be considered as transmission lines.

A transfer function representing these lines is derived in section 3.2. This function is shown to be directly frequency sensitive, and to contain some parameters which also are functions of frequency. The frequency sensitivity of the transmission lines and their representative lumped networks must be emphasized. A transient can be represented as a wave form or as a frequency specturm. A transient passing down a transmission line has its wave shape modified; the change can be analysed in terms of the transient's spectrum and the line's frequency response. Two devices with similar frequency response characteristics will have similar effects on transients passing through them. The purpose of this model is to duplicate the transient response of the large distribution system, so its components must have frequency responses matching those of the large system's components.

In section 3.3 an equivalent circuit is developed to duplicate the line's transfer function. With three elements, however, the equivalent

circuit is correct for only one frequency. One hundred kilocycles was the frequency chosen since all the lines could be simulated at this frequency and be approximate simulations at lower frequencies. If the results, based on the 100 kc model, indicate that higher frequencies may be important, the range of the model can be slightly extended, to about 500 kc. If still higher frequencies are required, the form of the equivalent circuit must be changed, and it will either be valid for high frequencies only, or will require extra elements. The effects of picking the 100 kc model are illustrated in section 3.4.

The equivalent circuits replace the cables in the system model shown in section 2.1.

3.2 Transmission Line Equations and Transfer Functions[1]

3.2.1. When a voltage, $E_g(t)$, is applied to the input terminals of a transmission line and a current is sent into the line, the voltage and resultant current are initially related by:

$$E(x) = I(x) \cdot Z_0 \qquad (3\text{-}1)$$

This is one of the solutions of "The telegraphers' equations":

$$\partial E/\partial x = -(I \cdot R + L \cdot \partial I/\partial t)$$
$$\partial I/\partial x = -(E \cdot G + C \cdot \partial E/\partial t)$$

Here R, L, C, and G are the distributed parameters of the transmission line, the values seen looking at a very short section of the line and considering it in relation to the relatively long, straight lines joined to it. Their units, typically, are:

R: ohms/meter L: henrys/meter

G: mhos/meter C: farads/meter

[1] This section is based on material from [12] and [16]

Taking x as the length down the line from the input terminals,

$$E(x) = E(0)\cdot e^{-\gamma x} = E(0)\cdot \exp(-\gamma x) \qquad (3\text{-}2)$$

Z_0 and γ are the transmission line constants, whose values depend on the lines' geometry and materials.[2] Z_0 is the line's surge impedance or characteristic impedance; γ is its propogation constant. The exponential term, in 3-2, is negative because the direction of power flow is in the direction of positive x, away from the source.

3.2.2. If the applied voltage is taken to be sinusoidal, of the form $E_g \cdot \exp(j\omega t)$ and if G is negligible, Z_0 and γ are given by:

$$Z_0 = \sqrt{\frac{R+j\omega L}{j\omega C}}, \text{ ohms} \qquad (3\text{-}3)$$

$$\begin{aligned} \gamma &= \sqrt{(R+j\omega L)(j\omega C)} \\ &= \frac{R+j\omega L}{Z_0} = (j\omega C)(Z_0) \\ &= \frac{1}{2}\left[\frac{R}{Z_0} + j\left(\frac{\omega L}{Z_0} + \omega C Z_0\right)\right] \\ &= \alpha + j\beta \end{aligned} \qquad (3\text{-}4)$$

$$\alpha \triangleq \frac{R}{2Z_0} \qquad (3\text{-}5\text{-}a)$$

$$\beta \triangleq \omega\left[\frac{L}{2Z_0} + \frac{CZ_0}{2}\right] \qquad (3\text{-}5\text{-}b)$$

If $\frac{\omega L}{R}$ is large (it is 30 or greater in the system being modeled)[1],

[2] Appendix B.4 shows their calculation.

[1] Table B.3, Appendix B.

$$Z_o \approx \sqrt{\frac{L}{C}} \qquad (3\text{-}5\text{-}c)$$

$$\beta = \omega\sqrt{LC} \qquad (3\text{-}5\text{-}d)$$

Now equation 3-2 can be written:

$$E(x,t) = |E(o,t)| \exp(j\omega t - j\omega\sqrt{LC}\,x - \alpha x) \qquad (3\text{-}6\text{-}a)$$

and,

$$|E(o,t)| = \left| \frac{Z_o}{Z_o + Z_g} \cdot E_g(t) \right| \qquad (3\text{-}6\text{-}b)$$

This shows that at time t, the voltage at x lags the voltage at x equal zero with phase angle equal to βx , and the magnitude has been attenuated in traveling from 0 to x by $\exp(-\alpha x)$. The same happens to $I(x,t)$.

If the input is other than sinusoidal, or if transients are of interest and Laplace transforms are going to be used:

$$Z_o = \sqrt{\frac{R+sL}{sC}}$$

$$\gamma = \sqrt{(R+sL)sC} = \frac{R+sL}{Z_o} = sCZ_o$$

With

$$Z_o \approx \sqrt{L/C}\,, \qquad \gamma = \alpha + s\sqrt{LC}$$

Now, in transformed form, equation 3-2 is:

$$E(x,s) = E(o,s)\exp(-\alpha x)\cdot\exp(-sx\sqrt{LC})$$

Again, $\exp(-\alpha x)$ represents attenuation. The second exponential term now represents a time delay, showing there is a time lag equal to $\sqrt{LC}$ before an event at $x = 0$ has an effect at distance x . A new quantity, v , the phase velocity is easily seen in this interpretation:

$$v = \frac{1}{\sqrt{LC}} \qquad (3\text{-}6\text{-}d)$$

This is the speed with which a wave travels down the line, and:

$$E(x,s) = E(0,s) \cdot \exp(-\alpha x - \frac{sx}{v}) \qquad (3\text{-}7)$$

In these, $E(0,s)$ is the transform of $\frac{Z_o}{Z_o+Z_g} \cdot E_g(t)$

3.2.3. Up to this point, a single wave of voltage and current has been pictured, traveling in one direction. The conditions governing it are the characteristic impedance and the propogation constant. Let this be called the forward wave, and subscript it with an f. At the end of the line there is, in general, a load with some impedance, Z_l. At this load, to the right of the l-terminals in Figure 3-1, this impedance defines the relation between voltage and current. But to the left of these terminals, Z_o relates them.

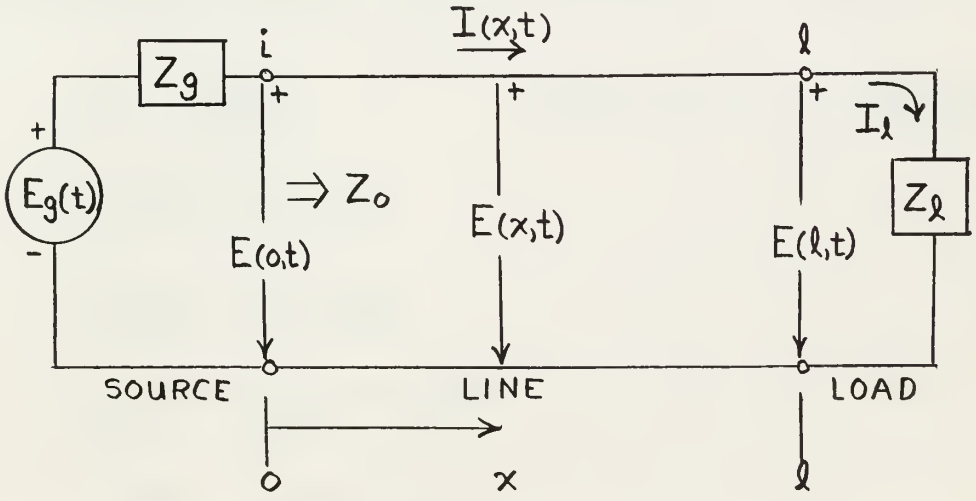

Figure 3-1

Transmission Line In a Circuit

Loosely speaking, if Z_ℓ is larger than Z_o, $I_f \cdot Z_\ell$ is larger than E_f, and an increase in voltage begins to propogate as a wave (with speed v) from the load toward the generator. Simultaneously, E_f/Z_ℓ is smaller than I_f, and a decrease in current is required, which propogates as a negative current wave. Conversely, if Z_ℓ is less than Z_o, I_f is too small for equilibrium and an increase in current propogates as a wave of positive current accompanied by a wave of negative voltage.

Speaking more precisely, at any time:

$$\begin{aligned} E_\ell &= I_\ell \cdot Z_\ell = E(x)\big|_{x=\ell} \\ I_\ell &= I(x)\big|_{x=\ell} \\ E_f(\ell) &= I_f(\ell) \cdot Z_o \end{aligned} \tag{3-8}$$

These requirements are met by adding the returning, or reflected, voltage and current waves, $E_r(\ell)$, $I_r(\ell)$, to the forward ones. The reflected waves are found from the load's coefficient of reflection, k_ℓ.

$$k_\ell = \frac{Z_\ell - Z_o}{Z_\ell + Z_o} \qquad \left(\text{magnitude} \leq 1 \text{ if } \Re\{Z_\ell\} \geq 0.\right)$$

$$\begin{aligned} E_r(\ell) &= k_\ell \cdot E_f(\ell) \\ I_r(\ell) &= -k_\ell \cdot I_f(\ell) \\ E(x) &= E_f(x) + E_r(x) \\ I(x) &= I_f(x) + I_r(x) \end{aligned} \tag{3-9}$$

The quantities determined by equations 3.9 satisfy the requirements of 3-8. The return waves propogate toward the generator with the same attenuation and delay per unit length but with:

$$E_r(x) = -Z_o \cdot I_r(x) \tag{3-10}$$

The distance traveled from ℓ to x is $\ell - x$, so $(\ell - x)$ replaces x in the exponent.

Taking the sinusoidal case,

$$E_r(x,t) = E_r(\ell,t) \cdot \exp(-\gamma(\ell - x))$$

$$= k_\ell \cdot E_f(\ell,t) \cdot \exp(-\gamma(\ell - x))$$

$$= k_\ell \cdot E(0,t) \cdot \exp(-\gamma\ell) \cdot \exp(-\gamma(\ell - x))$$

$$= k_\ell \cdot \left| E_g \frac{Z_o}{Z_o + Z_g} \right| \cdot \exp\left[j(\omega t - \beta(2\ell - x)) \right] \cdot \exp(-\alpha(2\ell - x))$$

showing the phase difference between the applied signal and the returning wave at any time, t, and distance, x. Similarly,

$$E_r(x,s) = k_\ell \cdot E(0,s) \cdot \exp\left[-\alpha(2\ell - x) - s\left(\frac{2\ell - x}{v}\right) \right] \qquad (3\text{-}11)$$

Note that if the applied voltage, $E_g(t)$, had included a switch or a unit step function, $U(t)$, the time expression found by inverting 3-11 would include a unit step, $U\left(t - \frac{2\ell - x}{v}\right)$.

With time, t, less than $2\ell/v$, at x on the line there is:

$$E(x,s) = E(0,s)\left[\exp\left(-x\left(\alpha + \frac{s}{v}\right)\right) + k_\ell \cdot \exp\left(-(2\ell - x)\left(\alpha + \frac{s}{v}\right)\right) \right]$$

$$I(x,s) = \frac{E(0,s)}{Z_o}\left[\exp\left(-x\left(\alpha + \frac{s}{v}\right)\right) - k_\ell \cdot \exp\left(-(2\ell - x)\left(\alpha + \frac{s}{v}\right)\right) \right] \qquad (3\text{-}12)$$

The reflected wave reaches the input, i, terminals at $t = \frac{2\ell}{v}$, and again there is, in general, a mismatch and a coefficient of reflection, k_g, must be defined for the generator terminals. (A match occurs when the terminal impedance, Z_g or Z_ℓ is equal to Z_o and the reflection coefficient, k_g or k_ℓ is zero.)

$$k_g = \frac{Z_g - Z_o}{Z_g + Z_o} \qquad (3\text{-}13)$$

Now there is an additional wave traveling from the generator towards the load, which is subscripted f_2 while the original is f_1 :

$$E_{f2}(0,s) = k_g E_{r1}(0,s) = k_g k_\ell \cdot E_{f1}(0,s) \exp\left(-2\ell\left(\alpha + \frac{s}{v}\right)\right)$$

$$I_{f2}(0,s) = -k_g I_{r1}(0,s) = k_g k_\ell I_{f1}(0,s) \cdot \exp\left(-2\ell\left(\alpha + \frac{s}{v}\right)\right) \tag{3-14}$$

With t less than $\frac{3\ell}{v}$ and $\gamma = \alpha + \frac{s}{v}$,

$$E(x,s) = E_{f1}(x,s) + E_{r1}(x,s) + E_{f2}(x,s) \tag{3-15}$$

$$= E(0,s)\left[\exp(-\gamma x) + k_\ell \cdot \exp\left(-\gamma(2\ell - x)\right) + k_g k_\ell \exp\left(-\gamma(2\ell + x)\right)\right.$$

$$I(x,s) = \frac{E(0,s)}{Z_o}\left|\exp(-\gamma x) - k_\ell \exp\left(-\gamma(2\ell - x)\right) + k_g k_\ell \exp\left(-\gamma(2\ell + x)\right)\right.$$

At the i terminals, the current entering the line is the algebraic sum of the current waves and the terminal voltage is the algebraic sum of the voltage waves. To the left of these terminals, all conventional lumped, circuit conditions are fulfilled.

Before the notation becomes overwhelming, the conventions in use thouls be reviewed. An ideal voltage source (zero internal impedance), $E_g(t)$, is connected through a generator impedance, Z_g, to the i terminals. $E(0,t)$, equal to $\frac{Z_o}{Z_o + Z_g} E_g(t)$ is the fraction of that voltage seen at the terminals; $E_g(0,s)$ and $E(0,s)$ are the transforms of these quantities. $E(0,s)$ is the first forward wave, $E_{f1}(x,s)$ at $x = 0$. $E_i(s)$ is the sum of all the voltage waves at $x = 0$ and $I_i(s)$ is the sum of the current waves there. Likewise, $E_\ell(s)$ and $I_\ell(s)$ are the sums at $x = \ell$.

Any change in E_g affects E_i only through its effect on E_{f1} until the changed E_{f1} wave has gone to the end of the line and returned as E_{r1}.

The f_2 wave, reflected at the generator by the r_1 wave, eventually generates an r_2 wave, and the process goes on forever, with ever increasing attenuation.

At a time when there are an even number of waves present on the line (every forward wave can be matched to a returning one), the line voltage is:

$$E(x,s) = E(0,s)\Big[\exp(-\gamma x) + k_\ell \exp(-\gamma(2\ell - x)) + k_\ell k_g \exp(-\gamma(2\ell + x)) \ldots + k_\ell^n k_g^n \exp(-\gamma(2n\ell + x)) + k_\ell^{n+1} k_g^n \exp(-\gamma(2n\ell + 2\ell - x))\Big] \quad (3\text{-}16)$$

$(2n+1)^{th}$ term $\qquad$ $(2n+2)^{th}$ term

The terms can be grouped together as:

$$E(x,s) = E_f(x,s) + E_r(x,s) = \sum(\text{odd terms}) + \sum(\text{even terms}) \quad (3\text{-}17a)$$

with

$$E_f(x,s) = E(0,s)\Big[\exp(-\gamma\ell) + k_g k_\ell \exp(-\gamma(2\ell + x)) + \ldots + k_\ell^n k_g^n \exp(-\gamma(2n\ell + x))\Big] \quad (3\text{-}17b)$$

Each of the terms in 3-17b includes a delay which, when the equation is inverted into the time domain, makes that term equal to zero until the time is equal to or greater than $\frac{2n\ell + x}{v}$. Therefore n may be allowed to grow very large, and as it does,

$$E_f(x,s) = \frac{\exp(-\gamma x)}{1 - k_g k_\ell \cdot \exp(-2\gamma\ell)} \cdot E(0,s) \quad (3\text{-}18a)$$

Similarly,

$$E_r(x,s) = \frac{k_\ell \cdot \exp(-\gamma(2\ell - x))}{1 - k_g k_\ell \exp(-2\gamma\ell)} \quad (3\text{-}18b)$$

Also:

$$I_f(x,s) = \frac{E_f(x,s)}{Z_0} \qquad I_r(x,s) = \frac{-E_r(x,s)}{Z_0} \quad (3\text{-}19)$$

From these,

$$E(x,s) = \frac{\exp(-\gamma x) + k_\ell \exp(-\gamma(2\ell - x))}{1 - k_\ell k_g \exp(-2\gamma\ell)} \cdot E(0,s) \qquad (3\text{-}20)$$

$$I(x,s) = \frac{\exp(-\gamma x) - k_\ell \exp(-\gamma(2\ell - x))}{1 - k_\ell k_g \exp(-2\gamma\ell)} \cdot \frac{E(0,s)}{Z_0}$$

3.2.4 Setting $x = 0$ or to ℓ gives the values at the input or load:

$$E_i(s) = E(0,s) \frac{1 + k_\ell \exp(-2\gamma\ell)}{1 - k_g k_\ell \exp(-2\gamma\ell)}$$

$$I_i(s) = \frac{E(0,s)}{Z_0} \cdot \frac{1 - k_\ell \cdot \exp(-2\gamma\ell)}{1 - k_g k_\ell \exp(-2\gamma\ell)} \qquad (3\text{-}21)$$

$$E_\ell(s) = E(0,s) \frac{\exp(-\gamma\ell)(1 - k_\ell)}{1 - k_g k_\ell \cdot \exp(-2\gamma\ell)}$$

$$I_\ell(s) = \frac{E(0,s)}{Z_0} \cdot \frac{\exp(-\gamma\ell)(1 - k_\ell)}{1 - k_g k_\ell \cdot \exp(-2\gamma\ell)}$$

Rearranging these into a more convenient form, a voltage transfer function, a current transfer function, and an input impedance are defined:

$$A_v = \frac{E_\ell(s)}{E_i(s)} = \frac{1 + k_\ell}{\exp(\gamma\ell) + k_\ell \exp(-\gamma\ell)} = \frac{Z_\ell}{Z_\ell \cosh\gamma\ell + Z_0 \sinh\gamma\ell} \qquad (3\text{-}22)$$

$$A_i = \frac{I_\ell(s)}{I_i(s)} = \frac{1 - k_\ell}{\exp(\gamma\ell) - k_\ell \exp(-\gamma\ell)} = \frac{Z_0}{Z_0 \cosh\gamma\ell + Z_\ell \sinh\gamma\ell} \qquad (3\text{-}23)$$

$$Z_i = \frac{E_i(s)}{E_\ell(s)} = \frac{Z_\ell + Z_0 \tanh\gamma\ell}{Z_0 + Z_\ell \tanh\gamma\ell} \qquad (3\text{-}24)$$

Any two of these equations define the system to the right of the terminals in Fig. 3-1.

3.2.5 The trigonometric functions of $j\beta$ or $j\frac{\omega}{v}$ are now substituted for the hyperbolic functions of γ, using the following approximations, which are discussed in section 3.4.2.

With small α :

$$\sinh(\alpha+j\beta)\ell \approx j \sin \beta\ell = j \sin(\omega\ell/v)$$

$$\tanh(\alpha+j\beta)\ell/2 \approx j \tan(\beta\ell/2) = j \tan(\omega\ell/2v)$$

The three forms of the transfer functions are now in the sinusoidal, steady state, form. The voltage gain, equation (3.22), is now:

$$A_v = 1/(\cos \omega\ell/v + j Z_o/Z_\ell \sin \omega\ell/v) \qquad (3\text{-}25)$$

If the load is inductive, its impedance is $j\omega\ell$ and the voltage gain has the form:

$$A_v = 1/(\cos \omega\ell/v + Z_o/\omega L \sin \omega\ell/v$$

This function has a pole each time $\tan\frac{\omega\ell}{v} = -\frac{\omega\ell}{Z_o}$. This occurs once in the second and once in the third quadrant every time the electrical angle $\frac{\omega\ell}{v}$, varies through π radians. Each time, the value of $\frac{\omega\ell}{v}$ is closer to $\frac{n\pi}{2}$ or $\frac{3n\pi}{2}$ (n an odd integer). Fig. 3-2 explains this drift with increasing ω. The minimum magnitudes are when $\tan\frac{\omega\ell}{v} = \frac{Z_o}{\omega\ell}$, and show a similar drift. Fig. 3-3 shows this frequency response for the case in which $\frac{Z_o}{L}$ is larger than 1 ohm/henry. For a given ℓ and v and a bandwidth determined by ω_n (lower) and ω_m (upper), there will be m-n poles of A_v, where m and n are the largest integers such that:

$$m \leq \frac{\omega_m \ell}{v\pi} \qquad\qquad n \leq \frac{\omega_n \ell}{v\pi}$$

If the load was capacitive, there would be as many poles, but in the other quadrants.

Figure 3-2

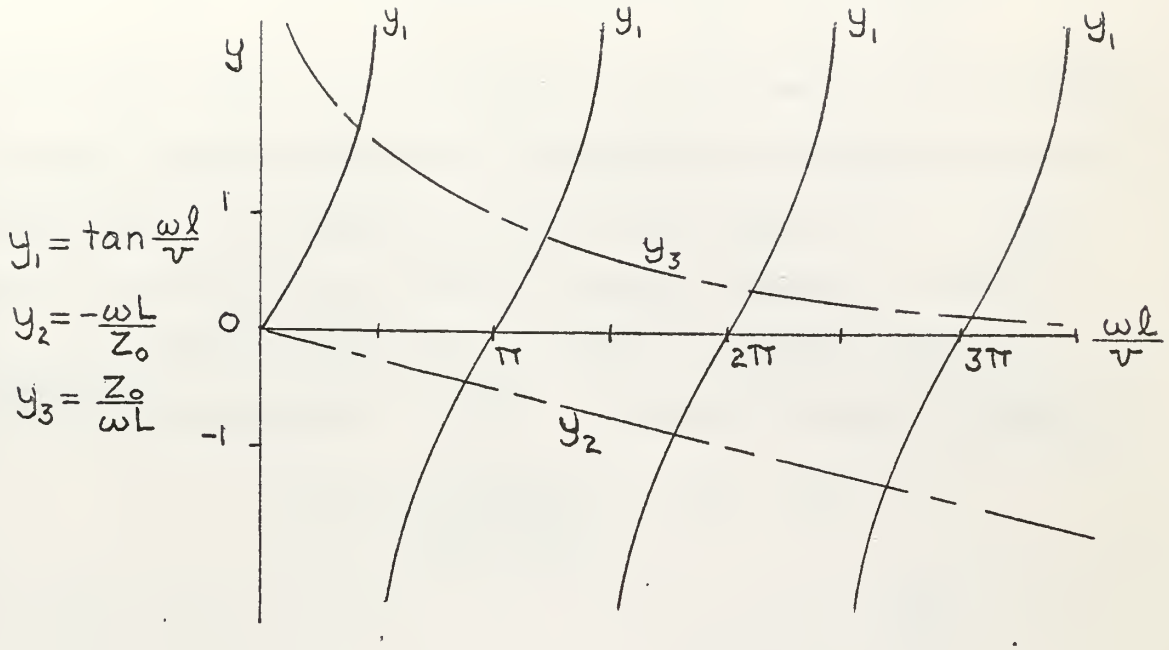

Illustrating the drift of the intersections of y_2 and y_3 with y_1.

Figure 3-3

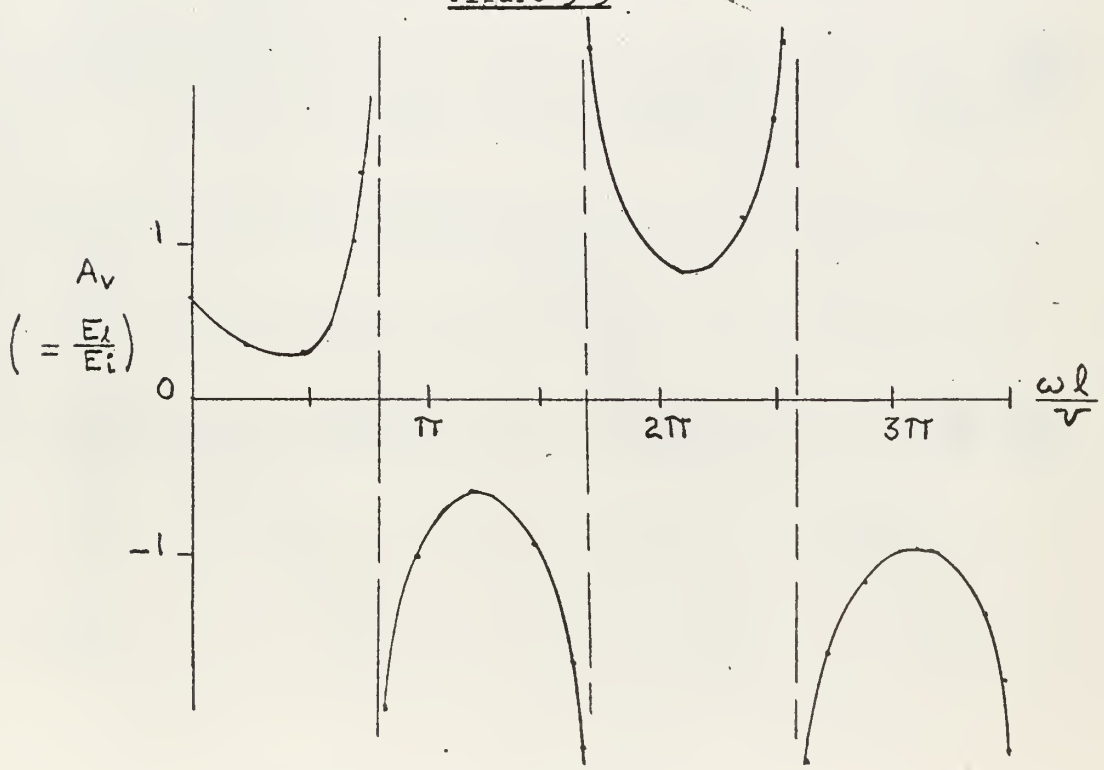

Voltage Gain With An Inductive Load

With a mixed load, $Z_\ell = R + j\omega L$ and:

$$A_V = \frac{R + j\omega L}{R\cos\frac{\omega\ell}{v} + j\left(\omega L\cos\frac{\omega\ell}{v} + Z_o\sin\frac{\omega\ell}{v}\right)}$$

As shown in Fig. 3-4, the magnitude of this function varies cyclically between a growing maximum and a minimum which rises from zero to unity asymptotically. The magnitude is equal unity to every π radians, and the phase angle varies clockwise from zero through $-\pi$ around to zero. The magnitude maxima occur when $\frac{\omega\ell}{v}$ is slightly greater than $\tan^{-1}\left(\frac{\sqrt{R^2+\omega^2L^2}}{Z_o}\right)$, the minima when $\frac{\omega\ell}{v}$ is slightly less than $\tan^{-1}\left(\frac{Z_o}{\sqrt{R^2+\omega^2L^2}}\right)$.

Figure 3-4
Magnitude and Phase of A_V With
An R-L Load

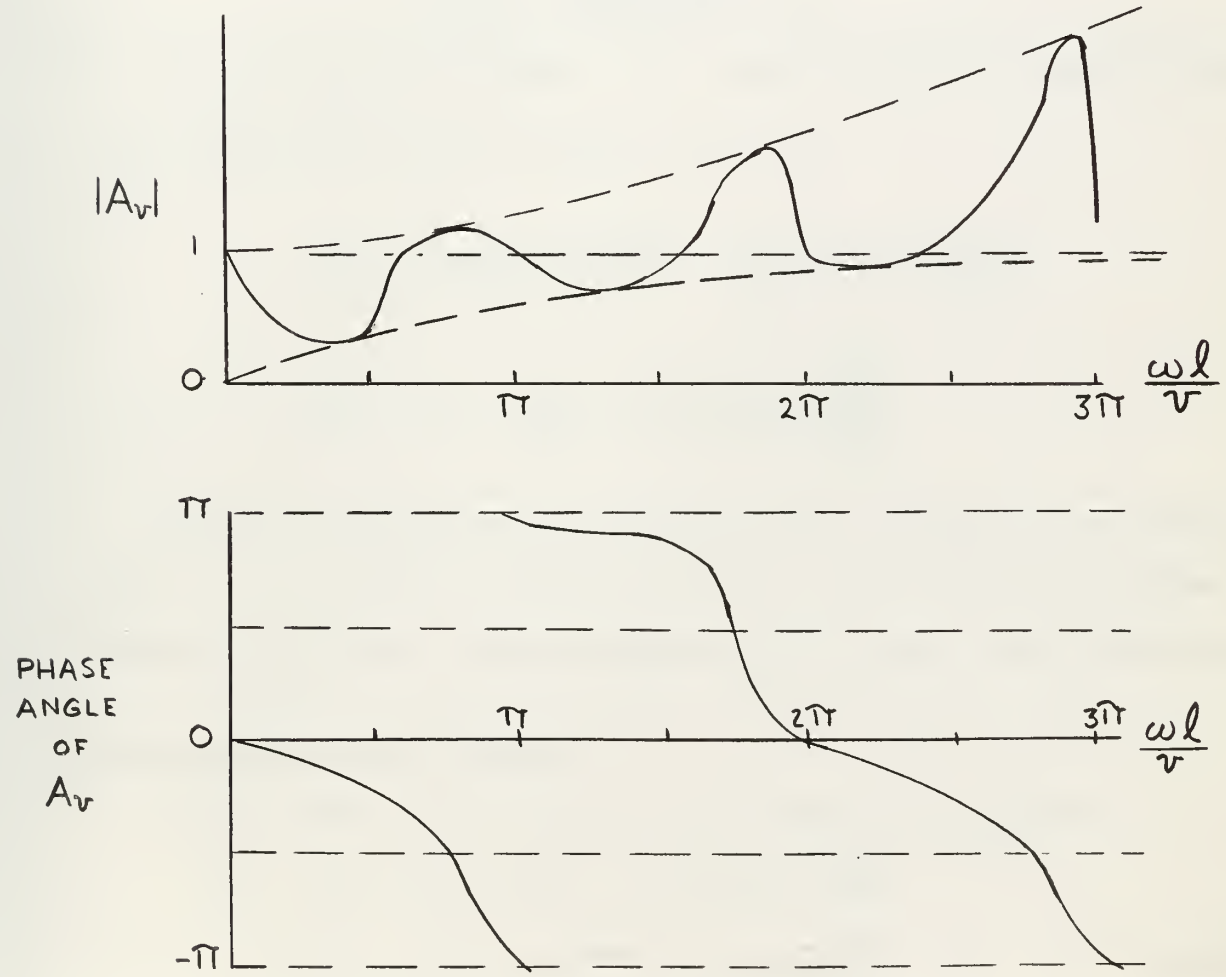

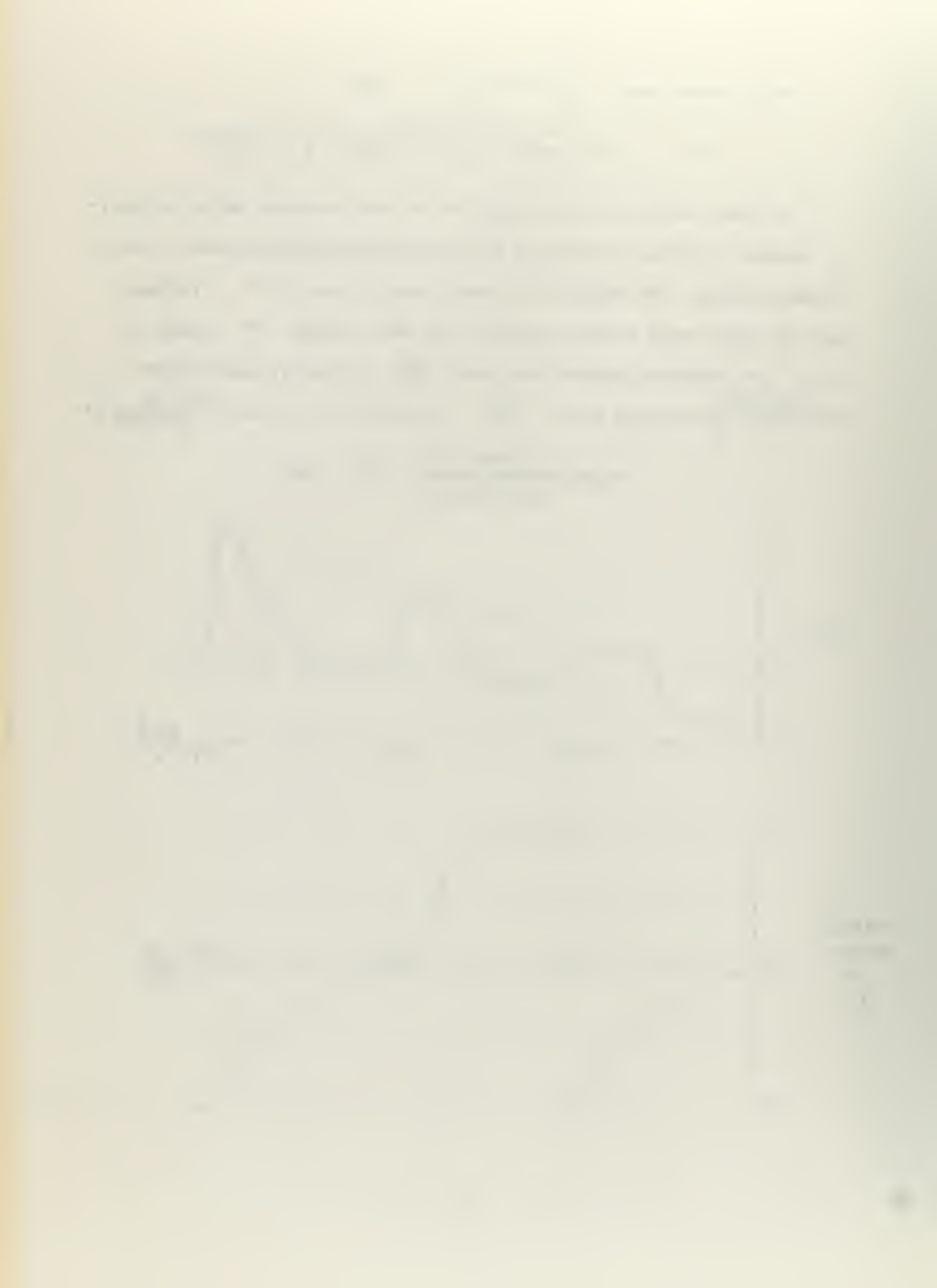

If the load is a simple resistance, the voltage transfer function is: $A_v = 1/(\cos\frac{\omega l}{v} + j\frac{Z_o}{R}\sin\frac{\omega l}{v})$ which is shown in Fig. 3-5.

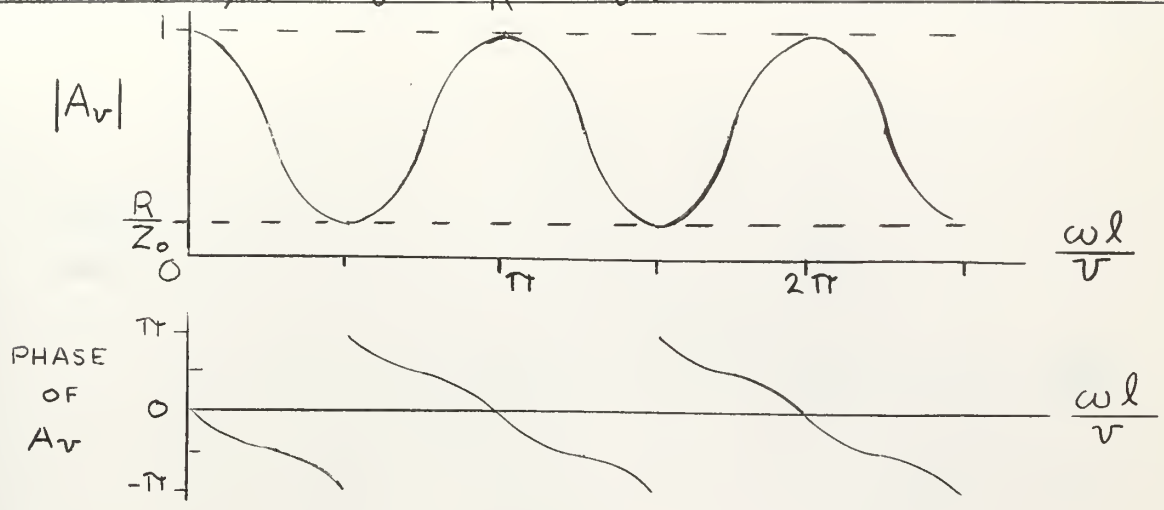

Figure 3-5
A_v with a Resistive Load

When the load is inductive, the current and impedance functions have the following form and are shown in Fig. 3-6.

$$A_i = 1/(\cos\frac{\omega l}{v} - \frac{\omega L}{Z_o}\sin\frac{\omega l}{v})$$

$$Z_i = j\,\frac{\omega L + Z_o \tan\frac{\omega l}{v}}{Z_o - \omega L \tan\frac{\omega l}{v}}$$

These three functions have been sketched to illustrate how they vary with ω. The effect of adding resistance to the load has been shown to dampen the function's extreme swings but not to make it less oscillatory.

3.3 Equivalent Lumped Network.

With a steady sinusoidal input, the transfer functions are:

$$A_v = Z_l/(Z_l\cos\frac{\omega l}{v} + j Z_o \sin\frac{\omega l}{v})$$

$$A_i = Z_g/(Z_o\cos\frac{\omega l}{v} + j Z_l \sin\frac{\omega l}{v}) \qquad (3\text{-}26)$$

$$Z_i = Z_o\,\frac{Z_l + j Z_o \tan\frac{\omega l}{v}}{Z_o + j Z_l \tan\frac{\omega l}{v}}$$

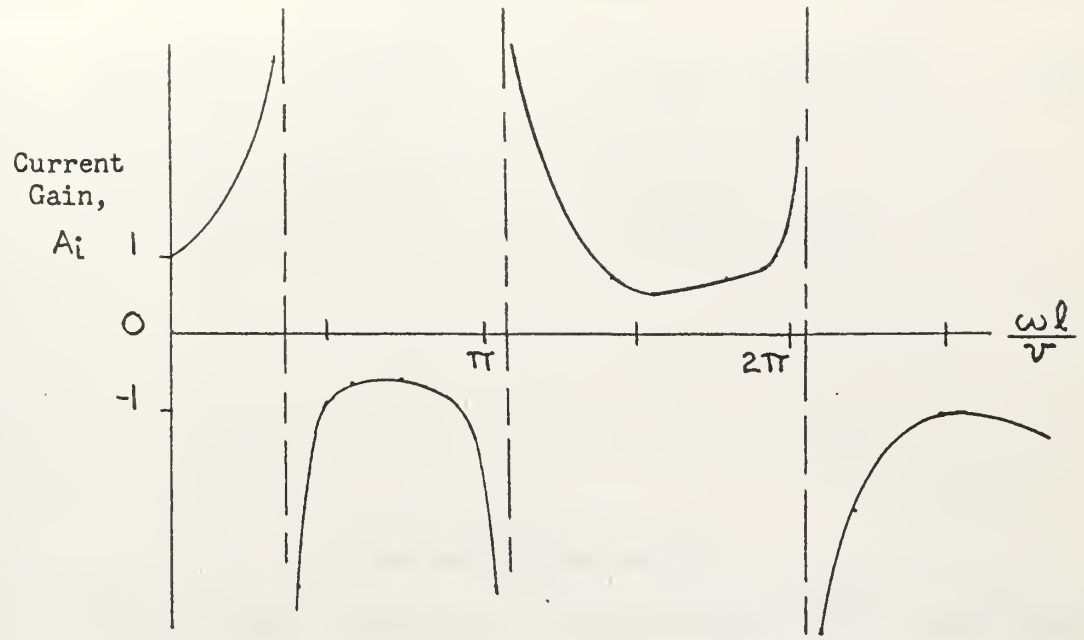

Figure 3-6

Current Gain and Input Impedance
With Inductive Load

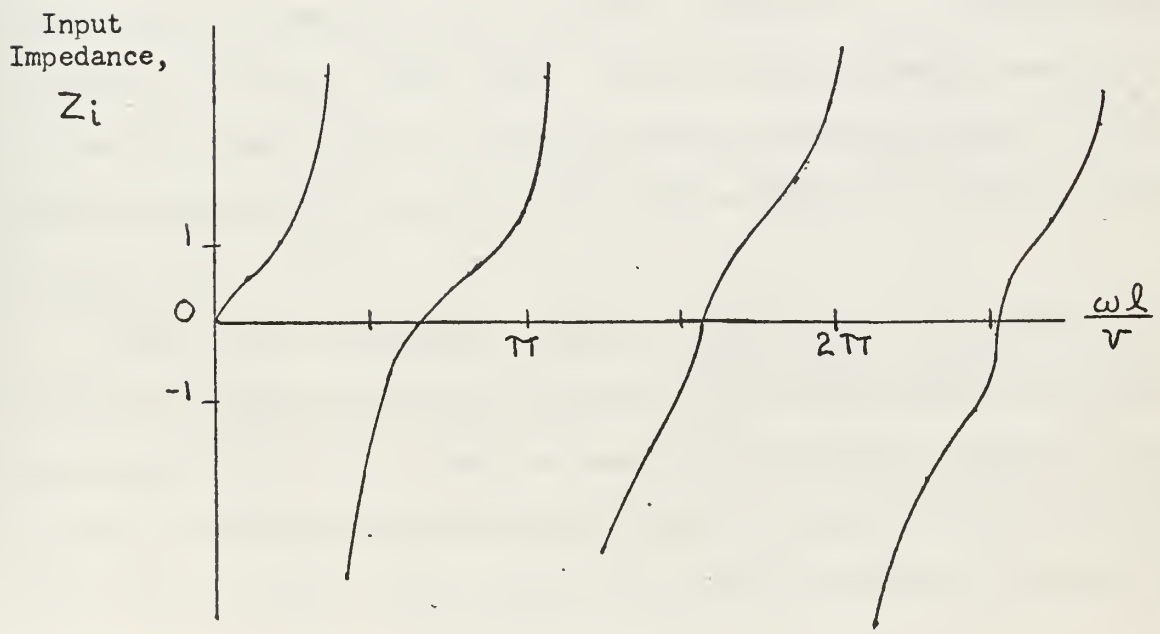

The network of Fig. 3-7 has the same transfer functions at one frequency, ω_1, if its elements are determined by the following equations

$$Z_s = j Z_o \tan \frac{\omega_1 \ell}{2v} \qquad Y_p = \frac{j \sin \frac{\omega_1 \ell}{v}}{Z_o} \tag{3-27}$$

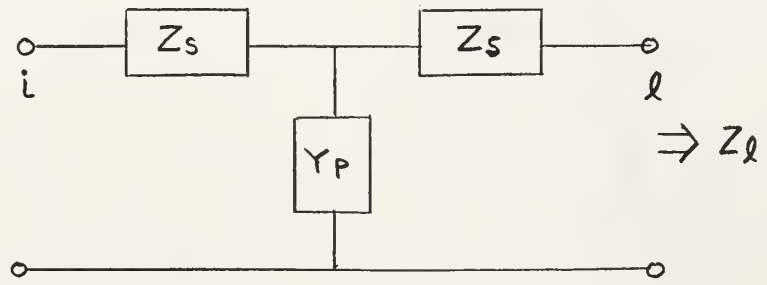

Figure 3-7
Equivalent Lumped Network

When the matching frequency is chosen so that $\frac{\omega_1 \ell}{v}$ is less than π, the series elements will be inductive and the parallel element will be a capacitor, with:

$$L_s = \frac{Z_o}{\omega_1} \tan \frac{\omega_1 \ell}{2v} \qquad C_p = \frac{\sin \frac{\omega_1 \ell}{v}}{\omega_1 Z_o} \tag{3-28}$$

The frequency response of such a network, connected to an inductive load, is shown in Fig. 3-8. When $\frac{\omega_1 \ell}{v}$ is in the third or fourth quadrants, the series elements will be capacitors and the paraller element an inductor. With the same load, the order of the transfer function is raised, as shown in Fig. 3-9.

There is not a convenient, explicit relationship between the equivalent circuit's transfer functions and those of the transmission line at frequencies other than ω_1. Even the poles are not usefully related. For instance, the input impedance pole of the L-C-L circuit (ω_3 in Fig. 3-8) can only be related to the transmission line's parameters by the equations

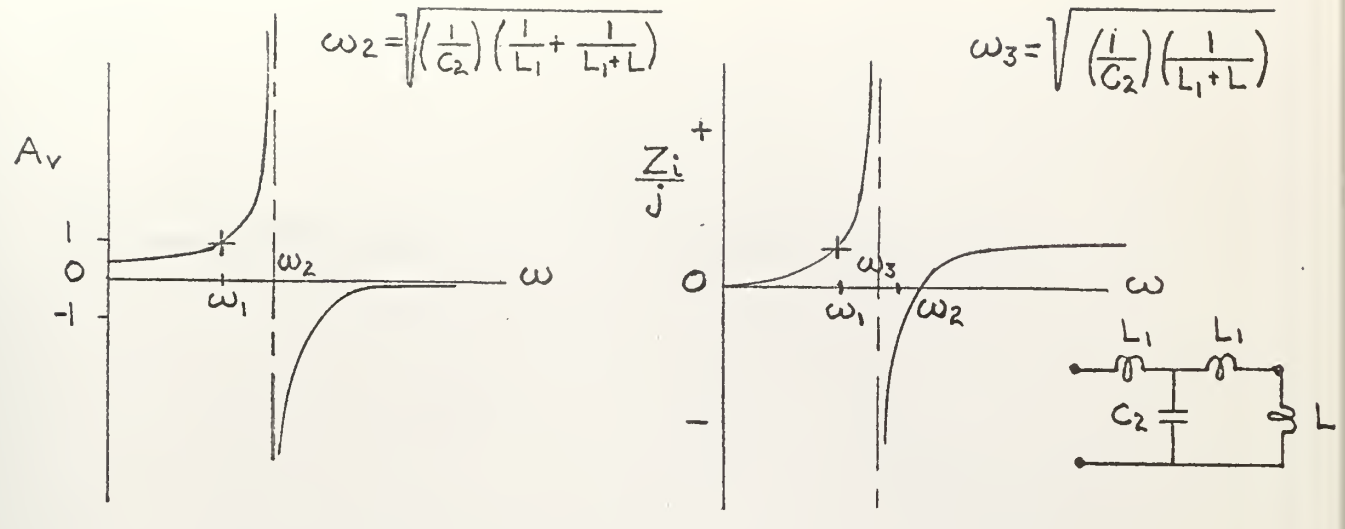

Figure 3-8

Voltage Transfer and Input Impedance of
The L-C-L Equivalent Lumped Network

$$\omega_{2,3} = \sqrt{\left(\frac{1}{C_1}\right)\left(\frac{1}{2L_2} + \frac{1}{L} \pm \sqrt{\frac{1}{4L_2^2} + \frac{1}{L^2}}\right)} \qquad \omega_4 = \sqrt{\frac{1}{C_1}\left(\frac{1}{L+L_2}\right)}$$

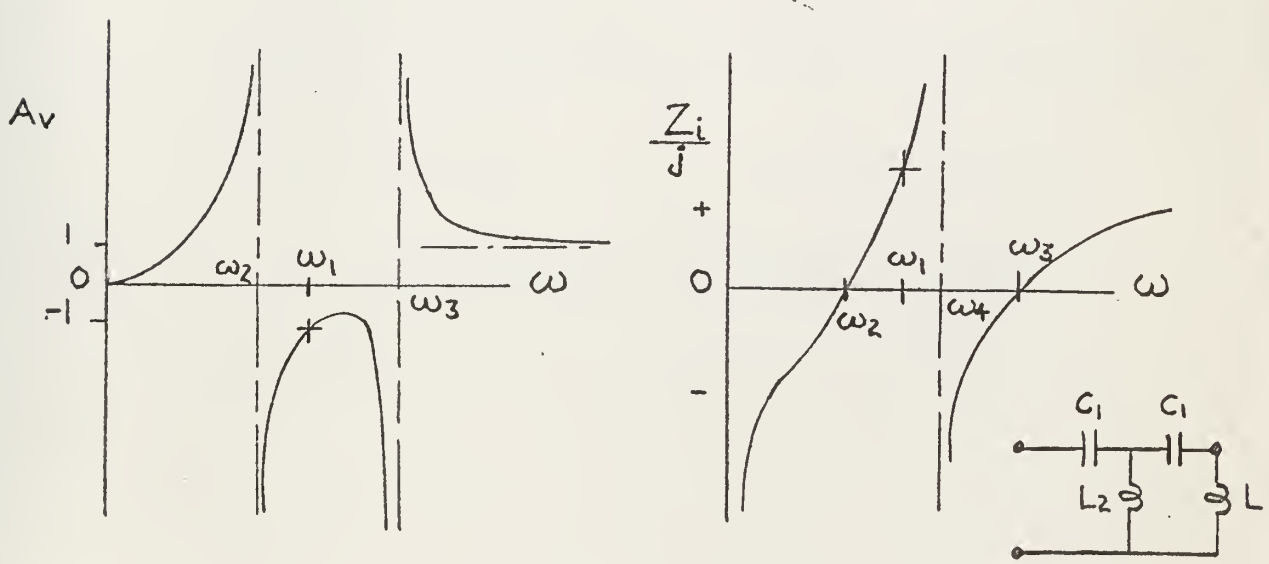

Figure 3-9

Voltage Transfer and Input Impedance of
The C-L-C Equivalent Network

circuit's A_V rises monotonically. The two are equal at ω_1. Over the lower frequency range, the two curves are bounded by two straight lines. It is because of these bounding values b_1 and b_2, illustrated in Fig. 3-10, that the L-C-L circuit is preferred.

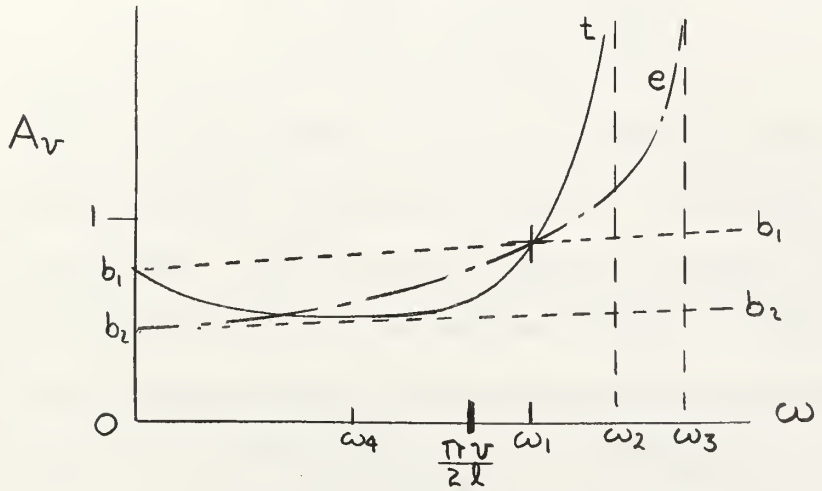

Figure 3-10
Comparison of Voltage Transfer Functions

t = transmission line's
e = lumped equivalent line's

b_1-b_1 is line from line's dc value to ω_1
b_2-b_2 is line from equivalent's dc value to line's minimum (ω_4) value.

$$\omega_2 = \frac{-Z_o}{L} \cdot \tan \frac{\omega_2 \ell}{v} \qquad \omega_4 = \frac{Z_o}{L} \cdot \cot \frac{\omega_4 \ell}{v}$$

$$\omega_3 = \omega_1 \sqrt{\frac{Z_o}{Z_o\left(1 - \cos \frac{\omega_1 \ell}{v}\right) + \omega_1 L \sin \frac{\omega_1 \ell}{v}}}$$

A more detailed analysis requires comparing numerical solutions for a particular line's parameters and for the equivalent circuit derived for a selected matching frequency. With this approach, an optimum equivalent could be defined and designed for a single line, but it is doubtful that such an optimum would be more meaningful than this procedure, picking a matching frequency and finding the equivalent for it, within specified limits.

3.4 Approximations.

3.4.1 Equations (3-22) and (3-24), repeated below, give the voltage transfer function and input impedance based on the wave equations.

$$A_v = Z_\ell / (Z_\ell \cosh \gamma\ell + Z_o \sinh \gamma\ell) \qquad (3\text{-}22)$$

$$Z_i = Z_o \cdot \frac{Z_\ell + Z_o \tanh \gamma\ell}{Z_o + Z_\ell \tanh \gamma\ell} \qquad (3\text{-}24)$$

With the basic circuit of Fig. 3-1, where an ideal generator or source is connected through a generator impedance to the loaded transmission line, the load voltage, $E(\ell,t)$, can be related to the input voltage, $E_i(t)$, by the equations above and to the applied voltage, $E_g(t)$. Alternatively, equation 3-21 maybe taken as the starting point and the same result derived, that (in transformed form, with $\gamma\ell = \frac{s\ell}{v} = s\tau$:

$$E(\ell,s) = E_g(s) \left(\frac{Z_o}{Z_o + Z_g}\right) \frac{(1+k_\ell)\exp(-s\tau)}{(1-k_g k_\ell \exp(-2s\tau))} \qquad (3\text{-}28)$$

$$= \frac{E_g(s) \cdot Z_o \cdot \exp(-s\tau)}{Z_o + Z_g} (1+k_\ell)\left[1 + k_g k_\ell \cdot \exp(-2s\tau) + \ldots + (k_g k_\ell)^n \exp(-2ns\tau) + \ldots\right]$$

With the following values (those for line number 3 and with an assumed source and load,

$$\ell = 67.056 \text{ m} \qquad Z_g = R_g = 15\,\Omega \qquad Z_\ell = R_\ell = 50\,\Omega$$

$$L_{dist} = 0.3634 \frac{\mu hy}{m} \qquad C_{dist} = 2569 \frac{pf}{m}$$

the values of the parameters in equation (3-28) are

$$Z_o = 11.894\,\Omega \qquad k_g = 0.1159$$

$$v = 0.3273 \times 10^8 \frac{m}{sec} \qquad k_\ell = 0.61566$$

$$\tau = 2.0487 \times 10^{-6} \text{ sec}$$

$$\frac{E_\ell(s)}{E_g(s)} = (0.7144)\cdot\exp(-2.0487\times10^{-6})\cdot\sum_{n=0}^{m}\exp(-2n\cdot2.0487\times10^{-6}s)\cdot(0.0711)^n$$

If the input is applied through a switch, $E_g(t) = U(t)$, then $E_\ell(t)$ is as shown in Fig. 3-11a. As m gets very large, $E_\ell(t)$ approaches 0.7687 volts.

Using the equivalent circuit, the values are:

$$L_1 = 11.38\,\mu hy \qquad C_2 = 9.464\times10^{-8}\,f$$

and

$$\frac{E_\ell(s)}{E_g(s)} = \frac{4.07954\times10^{18}}{s^3 + 5.71171\times10^6 s^2 + 7.6482\times10^{12}s + 5.3034\times10^{18}}$$

$$= \frac{3.2828\times10^5}{s+4.188\times10^6} + \frac{8.8044\times10^{11} - 3.30\times10^5 s}{(s+7.62\times10^5)^2 + (8.28\times10^5)^2}$$

Again, with a switched input,

$$E_\ell(t) = (.691) + (.078)\left[1 - \exp(-t/2.39\times10^{-7})\right]$$

$$-(.945)\left[\exp(-t/1.31\times10^{-6})\right]\sin(8.28\times10^5 t + 1.08)$$

$$-(.399)\left[\exp(-t/1.31\times10^{-6})\right]\sin(8.28\times10^5 t)\,.$$

which is shown in Fig. 3-11b.

Figure 3-11 shows the resemblance between the instantaneous response of the lumped element equivalent circuit and the delay-and-reflection response of the actual transmission line. If the equivalent circuit's frequency response could match the transmission line's at higher frequencies, there would be even greater similarity.

Figure 3-11
Comparison of Response to U(t) Input

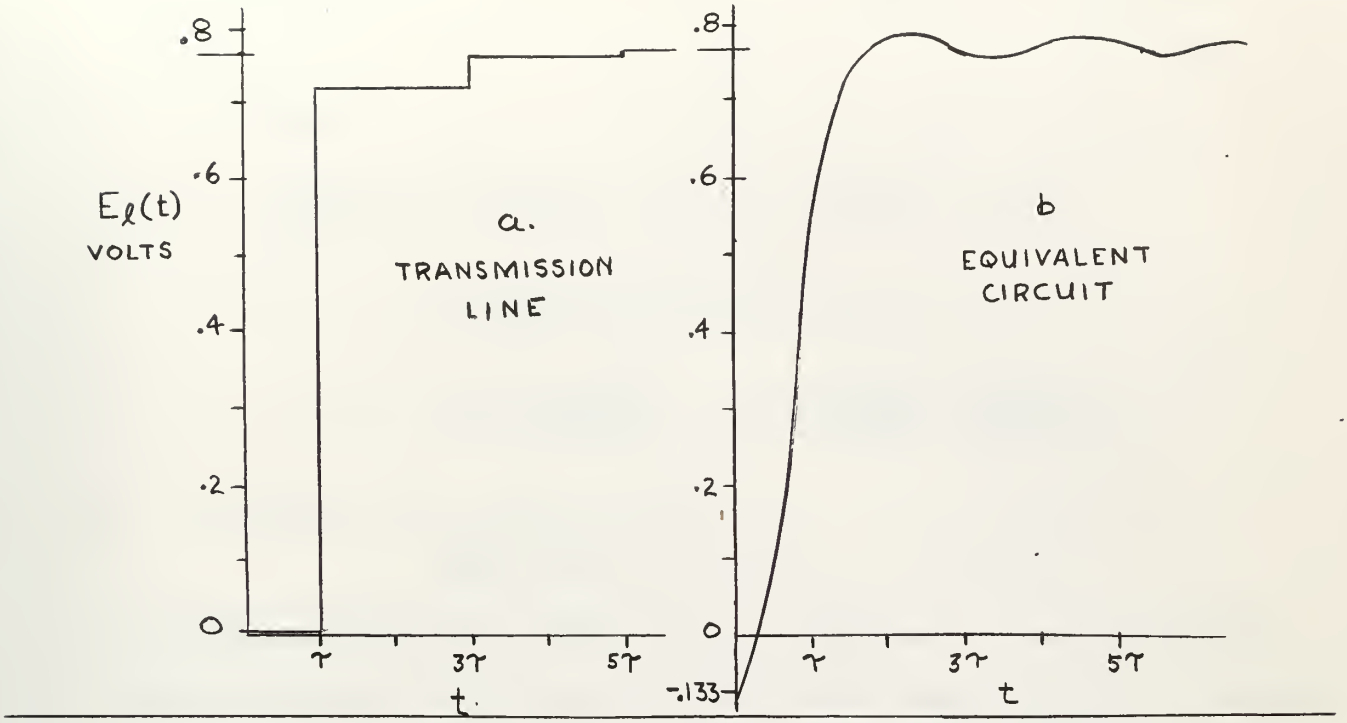

3.4.2 The replacement of the hyperbolic functions in section 3.2.5 is justified by the following. $\gamma = \alpha + j\beta$

$$\tanh\frac{\gamma\ell}{2} = \frac{(\sinh\gamma\ell)}{(\cosh\gamma\ell + 1)} = \frac{\sinh(\alpha\ell + j\beta\ell)}{1 + \cosh(\alpha\ell + j\beta\ell)}$$

$$= \frac{\sinh\alpha\ell\cdot\cos\beta\ell + j\cosh\alpha\ell\cdot\sin\beta\ell}{1 + \cosh\alpha\ell\cdot\cos\beta\ell + j\sinh\alpha\ell\cdot\sin\beta\ell}$$

$$= \frac{\sqrt{\sinh^2\alpha\ell + \sin^2\beta\ell}}{\cosh\alpha\ell + \cos\beta\ell}\angle\phi\,, \quad \phi = \tan^{-1}\left(\frac{\sin\beta\ell}{\sinh\alpha\ell}\right)$$

For small $\alpha\ell$, $\sinh\alpha\ell \approx \alpha\ell$ and $\cosh\alpha\ell \approx 1$

(for example: $\sinh .1 = .1002$
$\cosh .1 = 1.005$

so that when $\sin\beta\ell \gg \alpha\ell$, $\phi \approx 90°$, and $A\angle\phi = jA$

In the system under consideration, the smallest value of the ratio, $\frac{\sin\beta\ell}{\alpha\ell}$ with 100kc values, is 67.85 (Table B-3, Appendix B).

The statement that $\phi = 90°$, is in error by 0.84° in the worst case. The real part of A, equal to 1.48% of its magnitude, is being discarded.

Similarly:

$$\sinh \gamma\ell = \sinh \alpha\ell \cdot \cos\beta\ell + j \cosh\alpha\ell \cdot \sin\beta\ell$$

$$= \sqrt{\sinh^2 \alpha\ell + \sin^2\beta\ell}\ \angle\theta$$

$$\theta = \tan^{-1}\left(\frac{\tan\beta\ell}{\tanh\alpha\ell}\right) = \tan^{-1}\left[\frac{\sin\beta\ell}{\sinh\alpha\ell} \cdot \frac{\cosh\alpha\ell}{\cos\beta\ell}\right] \approx 90°$$

As above:

$$\sqrt{\sinh^2 \alpha\ell + \sin^2\beta\ell}\ \angle\theta \approx j \sin\beta\ell$$

As $\sin\beta\ell$ goes toward zero, where the approximations are poorly justified, the approximations go to zero also, where their exact counterparts approach very small, real, values. The implication is that when d-c, steady state, conditions are considered, the equivalent-circuit model of the transmission lines would not play any part in the distribution of voltage and current throughout the circuit; when transient conditions are considered, the real lines would have a damping effect which the model doesn't show. The damping of the motor loads is an order of magnitude larger, however, and this more important effect is retained in the model.

3.4.3. When the equivalent distributed parameters of a length of line have been calculated, Section 3.3 derives an equivalent lumped circuit. With the following manipulation, a simpler method is shown for arriving at the values for the lossless L-C-L circuit's elements. From Equation 3-28:

$$L_S = \frac{Z_o}{\omega_1} \tan\frac{\omega_1 \ell}{2v} \qquad C_P = \frac{1}{Z_o \omega_1} \sin\frac{\omega_1 \ell}{v}$$

where L_S and C_P are the series and parallel elements of the equivalent circuit: ω_1 is the match frequency, ℓ is the line's length, and Z_o is the lines' characteristic impedance. From 3-5-b and 3-6-d: $Z_o = \sqrt{L/C}$, $v = \sqrt{\frac{1}{LC}}$

where L and C are the distributed parameters.

Therefore:

$$L_S = \frac{Z_o \ell}{2v} \cdot \frac{\left(\tan \frac{\omega_1 \ell}{2v}\right)}{\left(\frac{\omega_1 \ell}{2v}\right)} = \frac{\ell L}{2} \cdot \frac{\left(\tan \frac{\omega_1 \ell}{2v}\right)}{\left(\frac{\omega_1 \ell}{2v}\right)} \qquad (3\text{-}30)$$

$$C_P = \frac{\ell}{v Z_o} \frac{\left(\sin \frac{\omega_1 \ell}{v}\right)}{\left(\frac{\omega_1 \ell}{v}\right)} = \ell C \frac{\left(\sin \frac{\omega_1 \ell}{v}\right)}{\left(\frac{\omega_1 \ell}{v}\right)}$$

If the loads terminating the line had a very small resistance, so that the lines' attenuation was an important part of the model, a series resistance could be found from equation (3-27) with $\tanh \frac{\gamma \ell}{2}$ replacing $j \tan \frac{\omega \ell}{v}$ or $j \tan \beta \ell$.

At the matching frequency:

$$Z_S = R_S + j\omega_1 L_S = Z_o \tanh \frac{\gamma_1 \ell}{2}$$

$$Z_o = \sqrt{\frac{R + j\omega_1 L}{j\omega_1 C}}, \quad \gamma = \sqrt{(R + j\omega_1 L)(j\omega_1 C)}$$

so $$\frac{Z_o \cdot \gamma \cdot \ell}{2} = \frac{\ell}{2}(R + j\omega_1 L)$$

and $$R_S = \frac{R\ell}{2} \frac{\tanh \frac{\gamma \ell}{2}}{\frac{\gamma \ell}{2}} \approx \frac{R\ell}{2} \frac{\tan \frac{\omega_1 \ell}{2v}}{\frac{\omega_1 \ell}{2v}}$$

If the matching frequency is taken as zero, then $L_S = \frac{\ell L}{2}$, $R_S = \frac{R\ell}{2}$ and $C_P = \ell C$. A comparison of the voltage transfer function of this

equivalent circuit and of the transmission line is shown in Fig. 3-12. The pole, ω_z , of the equivalent circuit has moved to the left of where it was in Fig. 3-10.

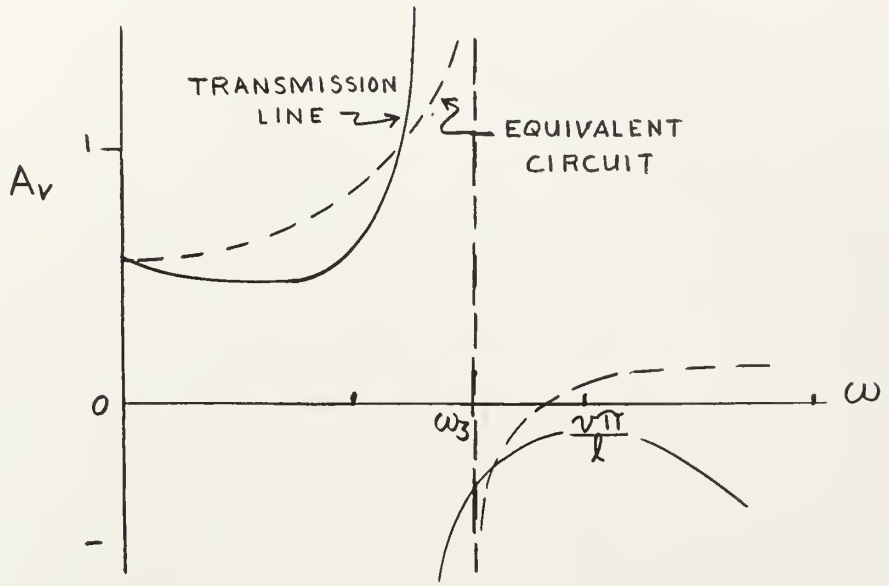

Figure 3-12
Voltage Transfer Functions with Zero Match Frequency

3.4.4 A basic assumption has been that the transmission line's distributed inductance and capacitance are independent of frequency. Or, in deriving the delay form-equation (3-18) - it has been assumed that L and C were independent of $\frac{dI}{dt}$ and $\frac{dE}{dt}$. But Appendix B shows that the distributed inductance varies with frequency because of the skin and proximity effects. Table B-1, summarizing this, shows that the d-c inductances of the system's cables are from 1.10 to 1.14 times as large as the 100 kc values. The rate of decrease, $-\frac{dL}{df}$ appears larger at low frequencies.

Z_o and $\frac{1}{v}$ are the two variables which have been emphasized in this

4. Electrical Circuit and Mathematical Description.

4.1 General.

The d-c distribution system is described in Section 2; circuit models of the various system components are developed in Section 3 and in Appendices B and C. The composite circuit model of the system is shown in Fig. 4-1. Although shown as a single line network with a common ground return, the ground is actually the electrical midpoint of a balanced circuit, as noted in Section 3.1. The T-sections which are the equivalents of the various cables are each designated by a single number in parenthesis; the number is the subscript identifying the L and C elements that make up the T. The lower case letters on the figure are used for node identification.

4.2 Mathematical Description.

4.2.1 Requirements.

The requirements imposed upon any model of the system, either breadboard or mathematical, are as follows:

a. The model should be sufficiently flexible to allow for additional loads and/or variation of the parameters of both loads and line.

b. Certain of the circuit nodes must be accessible, either as points at which the disturbance is initiated or as points of interest at which transients will be measured.

c. The model should permit application of various initial conditions at appropriate parts of the system.

d. If a mathematical model is to be used, it should be readily programmable for analog or digital computer solution.

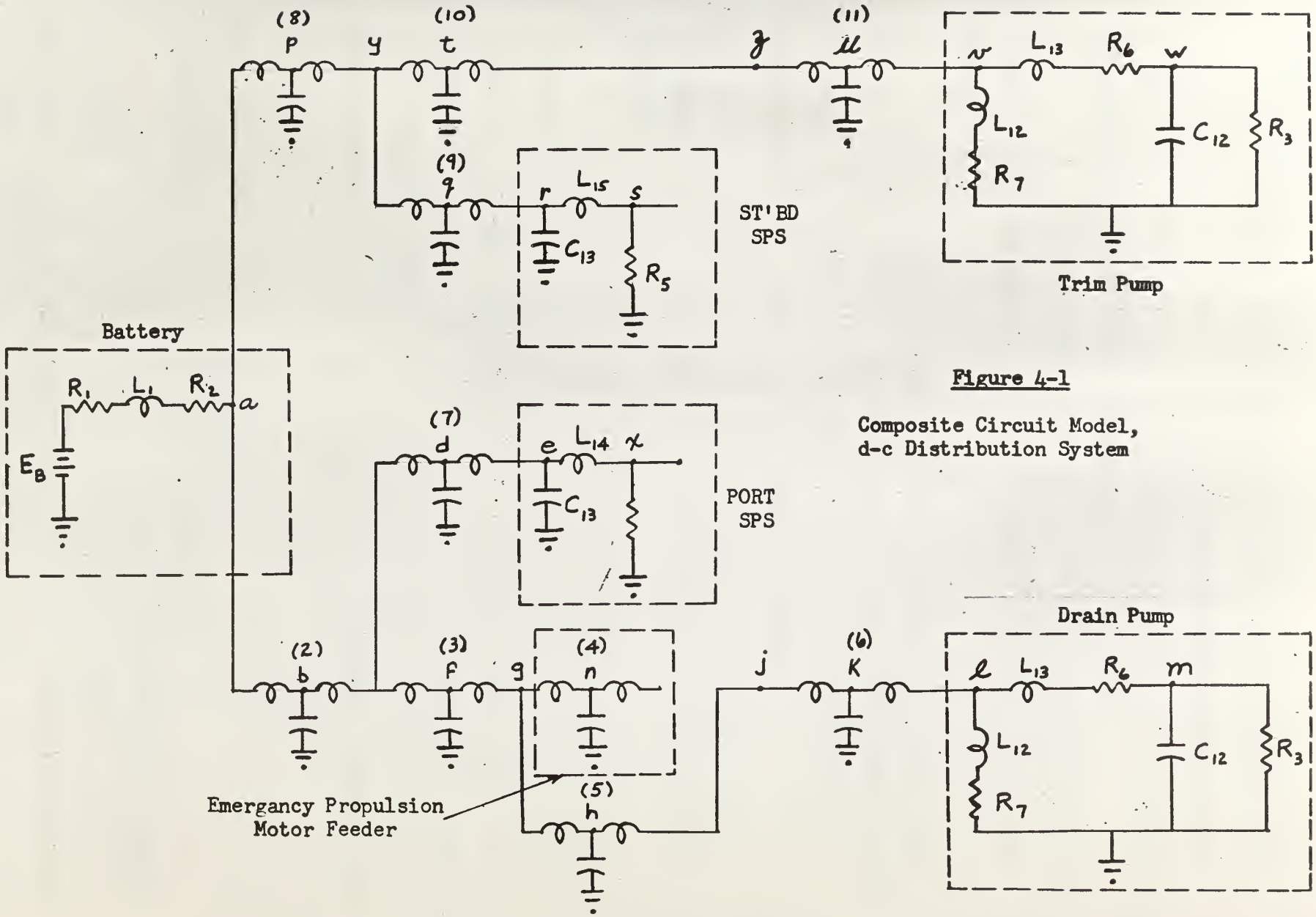

Figure 4-1

Composite Circuit Model,
d-c Distribution System

4.2.2. Signal Flow Graph.

The requirement of flexibility dictates against a breadboard model. A mathematical description which meets all of the above requirements and offers other advantages as well is the signal flow graph. The additional advantages offered by the flow graph are listed below:

a. It guards against algebraic redundancy in the formulation of inter-relationships between the many dependent variables of a large system.

b. It provides a visual check on the character of all closed paths. In a real, passive system the overall effect of any feedback must be negative. Therefore, at each node touched by one or more loops, at least one of the loops must develop negative feedback.

c. Each variable is visibly related to every other variable through a lattice of transmissions. Thus the effect of eliminating a dependent variable is readily apparent.

d. Small sections of a large network are easily isolated and simulated. By application of the rules for reducing the flow graph, a single-path transmission can be obtained, relating the variable of interest to the forcing function, and the behavior of the isolated section can be predicted analytically. By comparison of the simulation results and the analytical solution, the validity of the simulation technique may be verified.

4.3 Flow Graph of an Electrical Network.

4.3.1 Elementary Flow Graph Theory and Operations.

Sections 4.3.2 and 4.3.4 are largely tutorial regarding elementary concepts of linear flow graph theory as applied to passive electrical networks. All flow graph concepts presented herein are derived from reference [13] . For the reader already familiar with signal flow graphs, these

sections will serve to illustrate how the flow graph is applied in this study. Section 4.3.3 lists the polarity and subscripting conventions used.

4.3.2 Relationship of the Flow Graph to the Electrical Network.

No effort is made herein to develop the general theory of linear flow graphs, nor the circuit topology upon which the application of flow graphs to electrical circuits is based. These topics are comprehensively presented by S. J. Mason and Henry J. Zimmerman [13] . Only elementary concepts of flow graph theory are applied to the circuit of Fig. 4-1; these concepts are explained as they are applied.

The signal flow graph, as it is used herein, is a graphical representation of the set of simultaneous, linear differential equations that describe the inter-relationships of the circuit variables. The variables are the nodes of the graph; they are inter-connected by transmissions which express the dependence of a variable upon one or more of the other variables. At this point it is necessary to recognize the clear distinction between the nodes and branches of an electric circuit, and the nodes and transmissions of the flow graph describing the circuit. Circuit nodes are points at which two or more circuit elements (impedances, admittances, generators, etc.) have a common terminal; the circuit elements themselves comprise the branches. The nodes of the flow graph, on the other hand, are the circuit variables, usually current and voltage, which are inter-related by the graph transmissions. The functional dependence of node (variable) N_j upon the remaining variables is expressed by

$$N_j = \sum_i N_i T_{ij} \qquad (4\text{-}1)$$

where N_j is the source node of transmission T_{ij}.

Flow graphs may be used equally well with both loop and nodal analysis. The latter has been chosen as best suited to the requirements of the model, specifically, items b. and c. of Section 4.2.1 above.

4.3.3. Elementary Flow Graph.

For purposes of illustration the flow graph of a segment of the circuit of Fig. 4-1 will be developed. Fig. 4-2 shows the circuit to be considered; the node and circuit element designations correspond to those of Fig. 4-1.

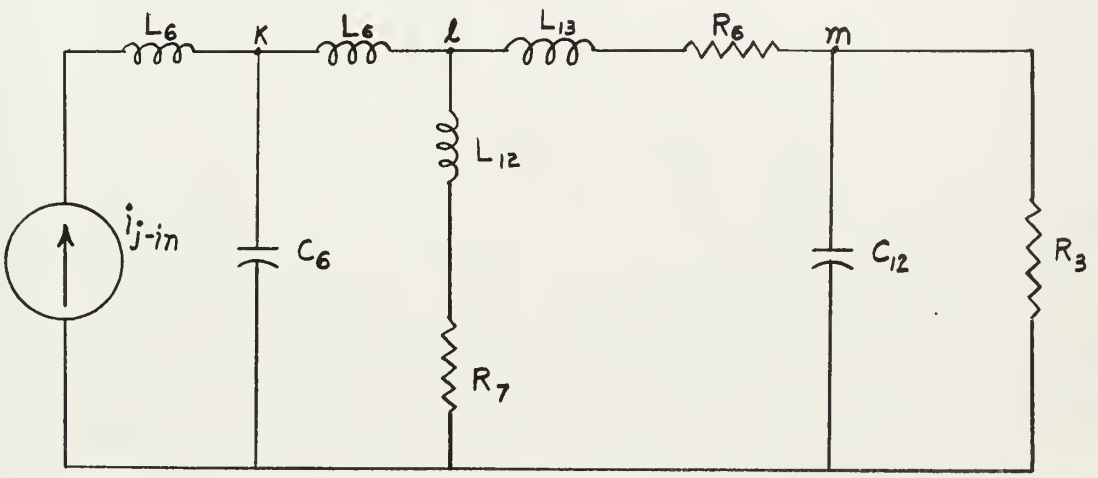

Figure 4-2
Illustrative Circuit

The polarity and subscripting convention followed through is as follows:

a. Positive currents enter nodes.

b. All node voltages are referred to the common electrical midpoint of the system, here shown as a common return.

c. The voltage subscript and the first letter of current subscripts indicate the node at which they are measured; the second

subscript on currents indicates the direction from which the current enters the node (a- above, b- below, 1 - left, r-right).

In formulating the flow graph for a given system it is usually not necessary to express the inter-relationships between the variables algebraically before diagraming them in the flow graph; indeed, it is generally redundant to do so. Such a procedure is followed in this development, however, so that the algebraic character of the flow graph is clearly established.

The transformed equations of the circuit of Fig. 4-2 follow:

$$I_{Kb} = -(I_{j\text{-}in} + I_{Kr}) \tag{4-2}$$

$$E_K = -I_{Kb}/sC_6 + e_K(0)/s \tag{4-3}$$

$$I_{Kr} = (E_\ell - E_K + i_{Kr}(0)L_6)/sL_6 \tag{4-4}$$

$$E_\ell = -(sL_{12} + R_7)I_{\ell b} + i_{\ell b}(0)L_{12} \tag{4-5}$$

$$I_{\ell b} = I_{Kr} - I_{\ell r} \tag{4-6}$$

$$I_{\ell r} = (E_m - E_\ell + i_{\ell r}(0)L_{13})/(sL_{13} + R_6) \tag{4-7}$$

$$E_m = -I_{mb}/sC_{12} + e_m(0)/s \tag{4-8}$$

$$I_{mb} = I_{\ell r} + E_m/R_3 \tag{4-9}$$

Note that the equations are formulated so that the functional relationship of each dependent variable is expressed explicitly once and only once. The flow graph of equations (4-2) through (4-9) is shown in Fig. 4-3.

4.3.4 Operations on the Signal Flow Graph

The flow graph of Fig. 4-3 is a complete analytical expression, relating each of the system's dependent variables to every other and to the forcing functions - the initial conditions and the independent variable, $I_{j\text{-}in}$. For computer simulation, however, further operations on the

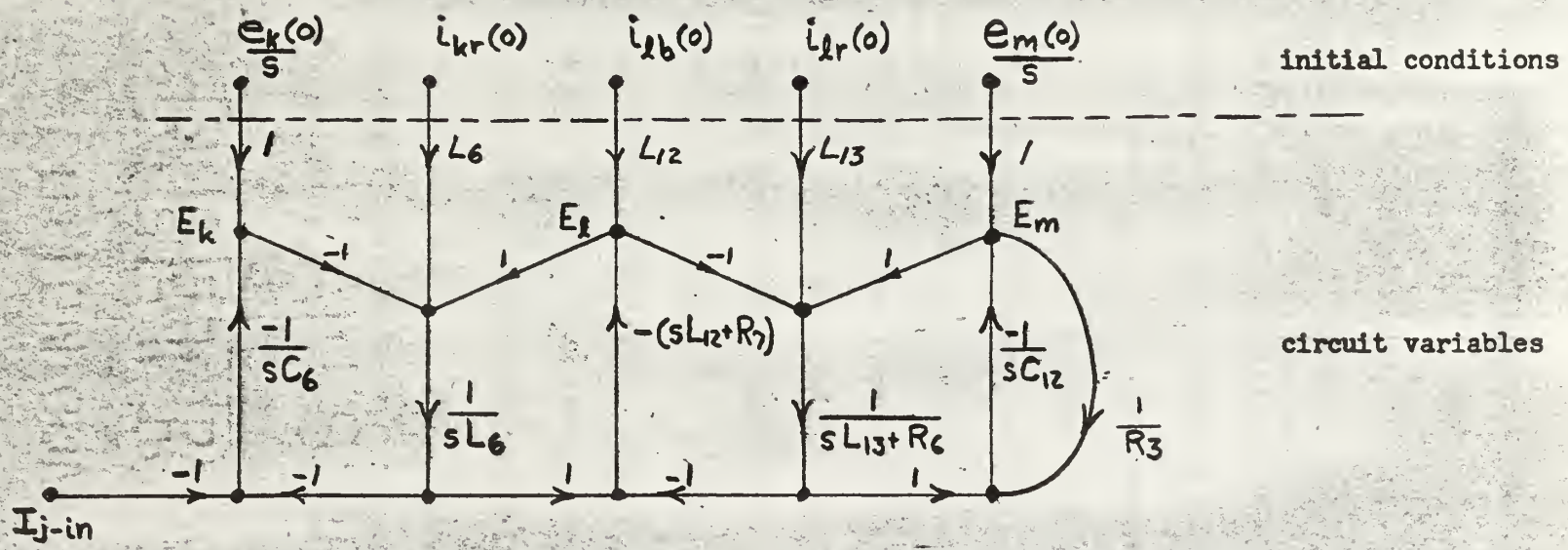

Figure 4-3

Signal Flow Graph of Illustrative Circuit

flow graph are desirable.

In equation (4-5) and the corresponding transmission of the flow graph the term $-(sL_{12}+R_7)I_{lb}$ appears; this implies a time differentiation of $i_{lb}(t)$. Differentiators should be avoided where possible. In electronic analog computers, internal noise causes wide voltage excursions across amplifiers used as differentiators. Numerical differentiation has inherent limitations which render its use inadvisable. [10] By absorption of the node E_l, the transmissions from I_{lb} to I_{Kr}, and from I_{lb} to I_{lr} can be expressed without the differentiators. Absorbing a signal flow graph node corresponds exactly to the elimination of a variable from the corresponding set of simultaneous equations. The governing concept in any transmission of the flow graph is, of course, that the total transmission between any two nodes, not absorbed in the transformation, must remain unaltered.

Figure 4-4 illustrates the transformation. In Fig. 4-4(a), E_l is absorbed. Direct transmissions from I_{lb} are given by the ratios, $-\frac{(sL_{12}+R_7)}{sL_6}$ and $-\frac{(sL_{12}+R_7)}{(sL_{13}+R_6)}$ The initial condition, $i_{lb}(0)L_{12}$, is shifted to each of the two nodes adjacent to E_1, which are partially dependent on that variable. In Fig. 4-4(b), each of the ratios formed in the previous operation, itself forms two transmissions - one is a gain, the other corresponds to a time integration.

The direct transmissions between the nodes of the pair (I_{Kr}, I_{lb}) form a closed gain loop, $-\frac{L_{12}}{L_6}$; similarly, a closed gain loop, $-\frac{L_{12}}{L_{13}}$, exists at the node pair (I_{lb}, I_{lr}). For reasons given in Section 5, such gain loops generate instabilities in some methods of simulation. These loops are removed by the successive transformations shown in Fig. 4-5. The essential character of these loops is preserved if they are

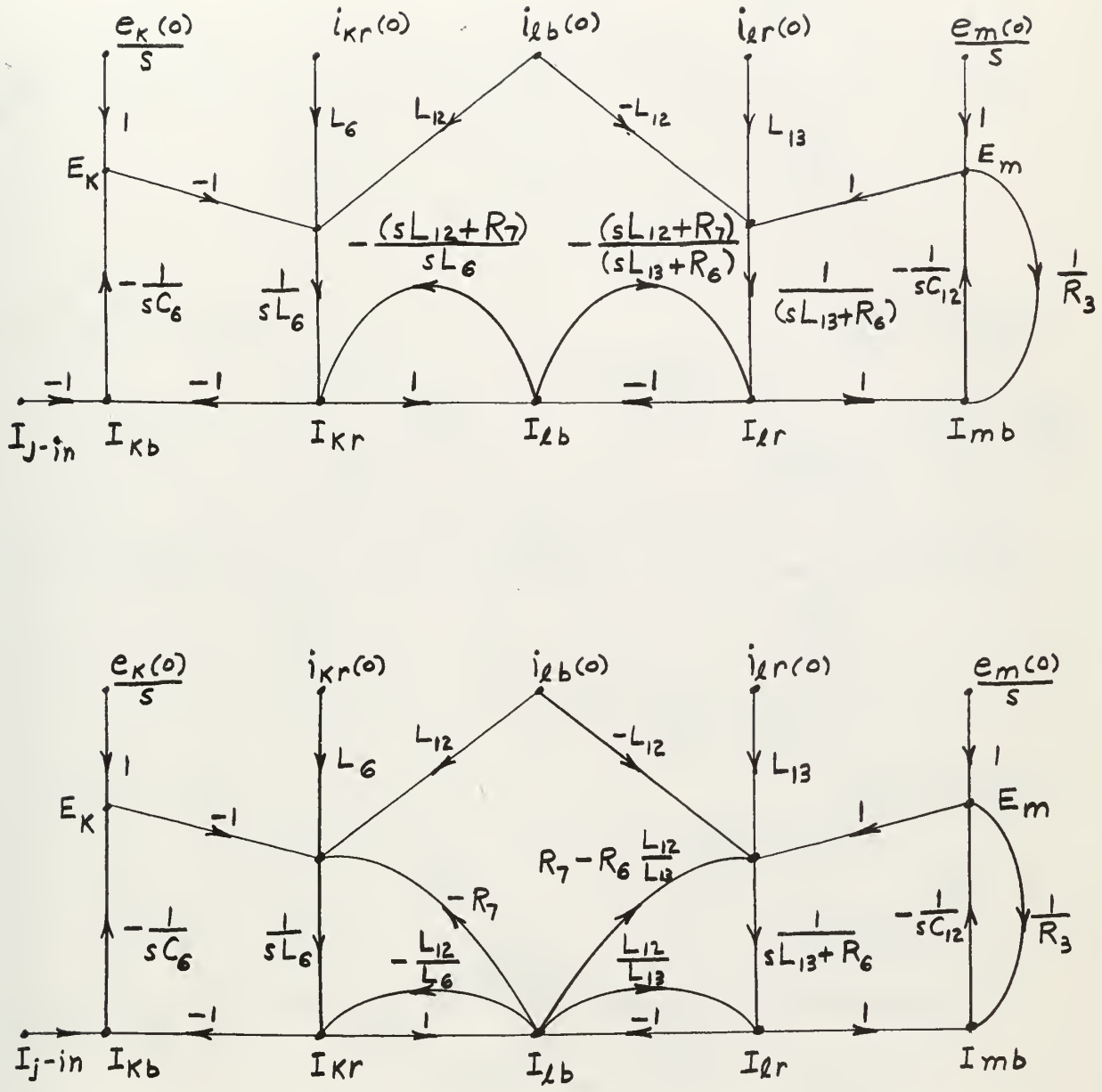

Figure 4-4

Removal of Differentiators

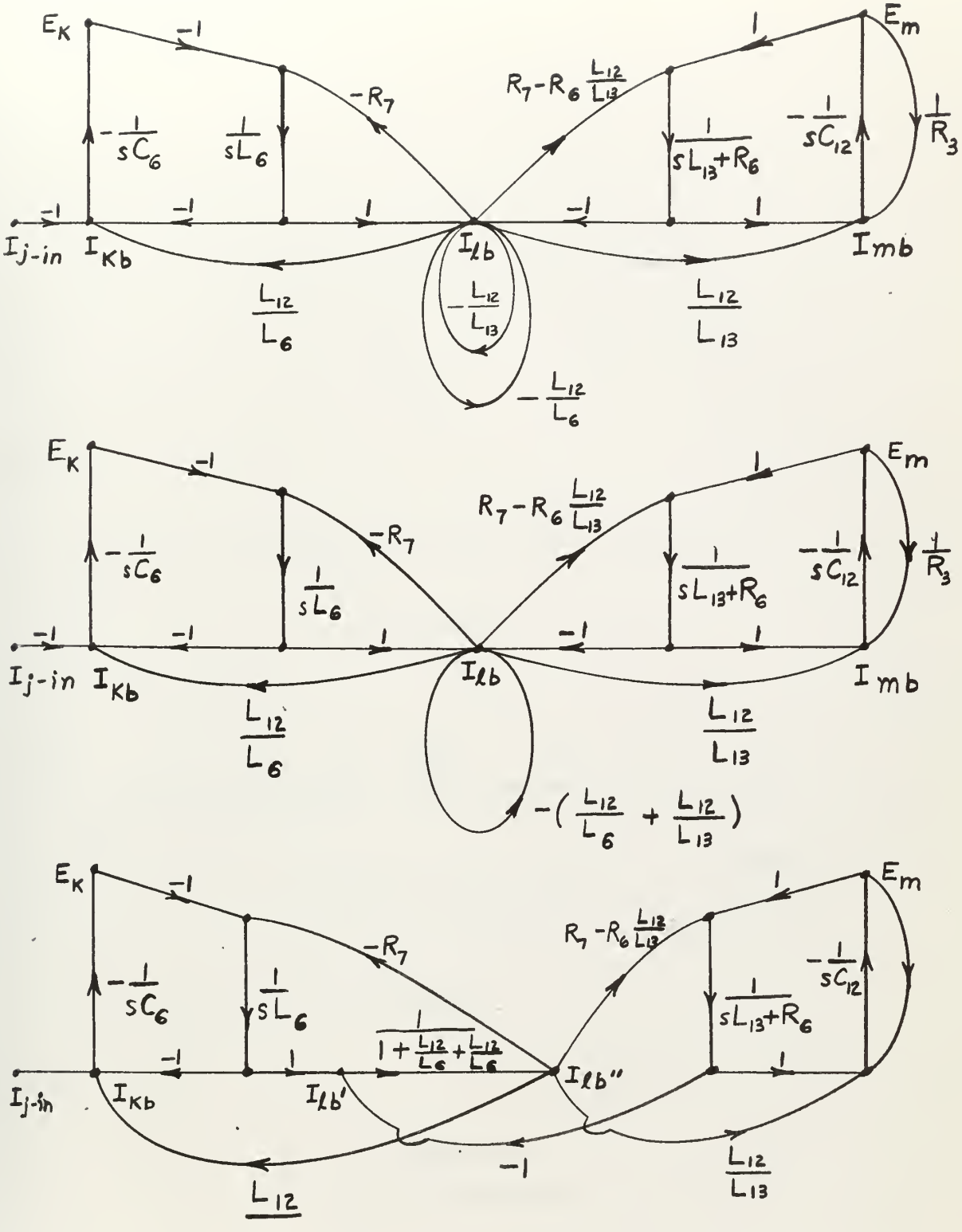

Figure 4-5

Removal of Gain Loops

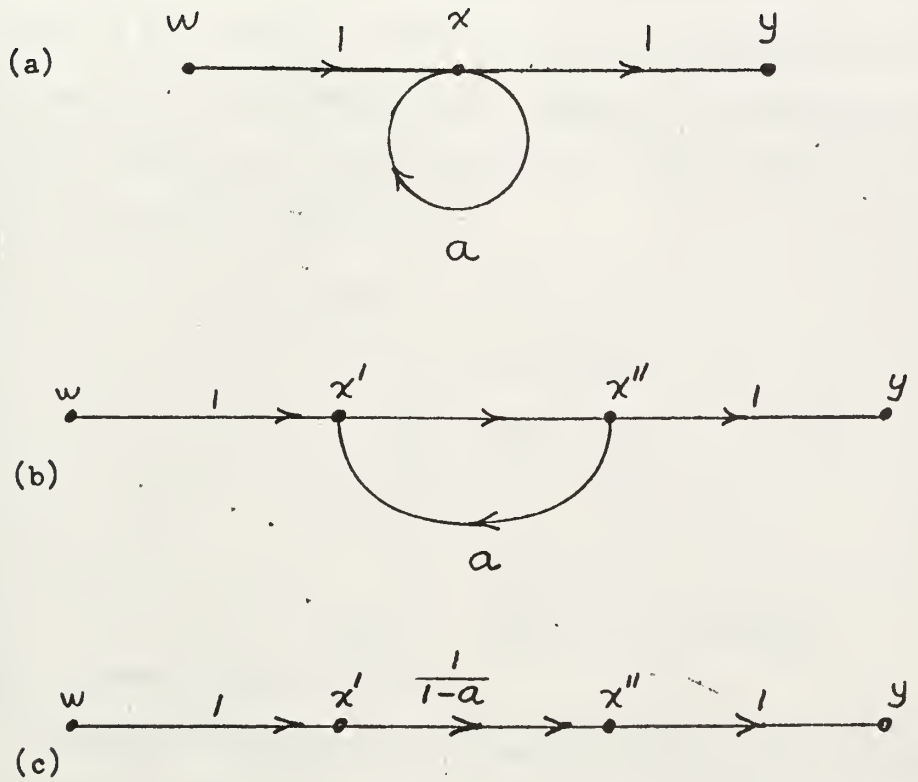

$$y = x + ax + a^2x + \cdots + a^nx + \cdots$$

$$= w(1 + a + a^2 + \cdots a^n + \cdots$$

$$= w \cdot \frac{1}{1-a}$$

Figure 4-6

Removal of Self-Loop

separated into a node-to-node transmission and a self-loop. This can be accomplished at either of the nodes touched by the loop. I_{Kb} was chosen as the node at which to establish both self-loops as is shown in Fig. 4-5(a). The self-loops at I_{Kb} are parallel transmissions and can therefore be added together to form the single self-loop illustrated in Fig. 4-5(b). The self-loop can be replaced by a node-to-node transmission of the proper form. Consider the flow graph of Fig. 4-6(a). By splitting node x into x' and x'' as in Fig. 4-6(b), the transmission T_{wy} is readily evaluated:

$$x' = w + a x'' \tag{4-12}$$

$$= w + a x' \tag{4-12a}$$

$$= w/(1-a) \tag{4-13}$$

$$y = x'' = x' \tag{4-14}$$

$$= w/(1-a) \tag{4-14a}$$

$$T_{wy} = y/w = 1/(1-a) \tag{4-15}$$

This is shown in Fig. 4-6(c).

A similar transformation of the self-loop of Fig. 4-5(b) yields the graph, Fig. 4-5(c), which can be used as a basic for simulating the circuit of Fig. 4-2 on either an electronic analog or digital computer.

4.3.5 Resume of Transformations.

By elementary flow graph transformations, certain transmissions have been eliminated which would have caused difficulty in computer simulation. In carrying out these transformations, however, certain nodes representing measurable system voltages or currents were necessarily eliminated. Similarly, new nodes, dimensionally equivalent to voltage or current, but not directly identifiable with a particular circuit voltage or current, were caused to appear. By continued repetition of the transformation

processes described in the preceding sections, further reduction of the flow graph is possible. The extent to which such transformations are carried out depends upon the degree of resemblance that is desired between the flow graph nodes and transmission and the parameters of the system being described. For purposes of this study the only transformations desired are those which remove differentiators or pure gain loops. The result is a flow graph which retains many of the circuit's node voltages and branch currents.

4.4 System Flow Graph

Observing the polarity and subscript conventions stated in 4.3.3 the circuit of Fig. 4-1 is described by the flow graph, Fig. 4-7. Correspondence of the circuit with segments (a) through (3) of the flow graph is as follows:

Fig. 4-7(a)	SPS - starboard
(b)	Trim Pump
(c)	SPS - port
(d)	Emergency Propulsion Feeder
(e)	Drain Pump

In order to keep the system flow graph relatively uncluttered, initial conditions are not shown in Fig. 4-7. They cannot be neglected, however, and should be applied as in the illustrative circuit described in 4.3.

The circled nodes of Fig. 4-7 are those common to two or more segments of the flow graph.

By processes described above, differentiators, gain loops, and self-loops are removed from the basic flow graph to yield the graph, Fig. 4-8.

All non-unity transmissions are labeled by one or two lower-case letters, and each node not otherwise identified in terms of circuit currents or voltages is assigned upper-case letters for reference. The transmissions are tabulated in Table 4-1. In Table 4-2 are listed all nodes of Fig. 4-8 to which initial conditions are applied, together with the initial conditions.

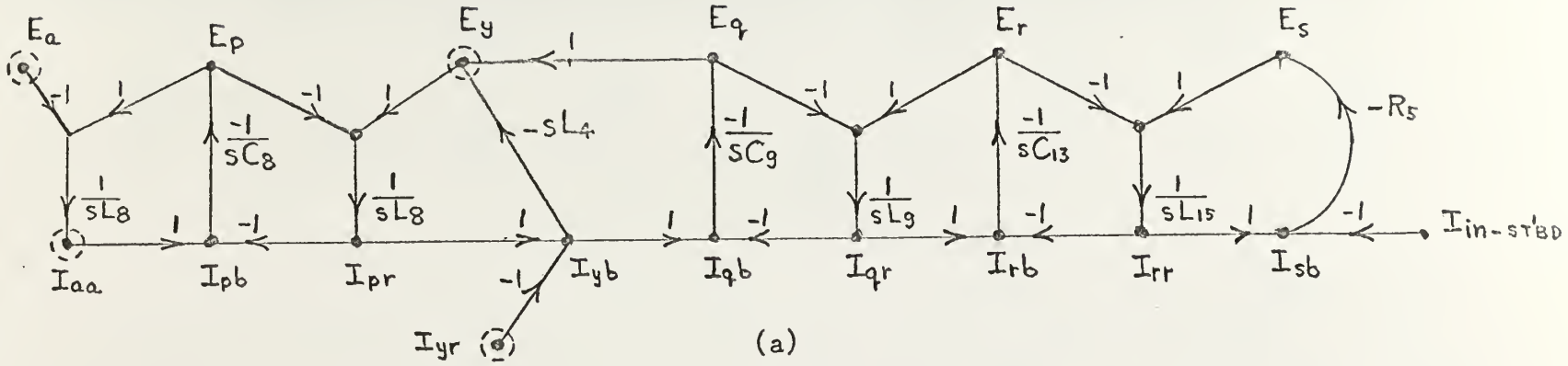

Figure 4-7
Basic Flow Graph of d-c System

(b)

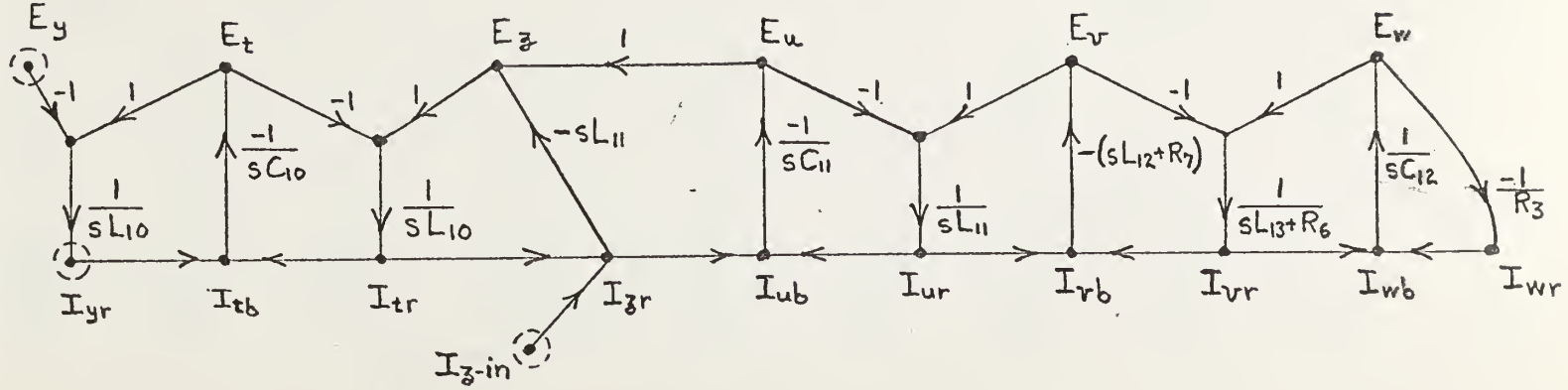

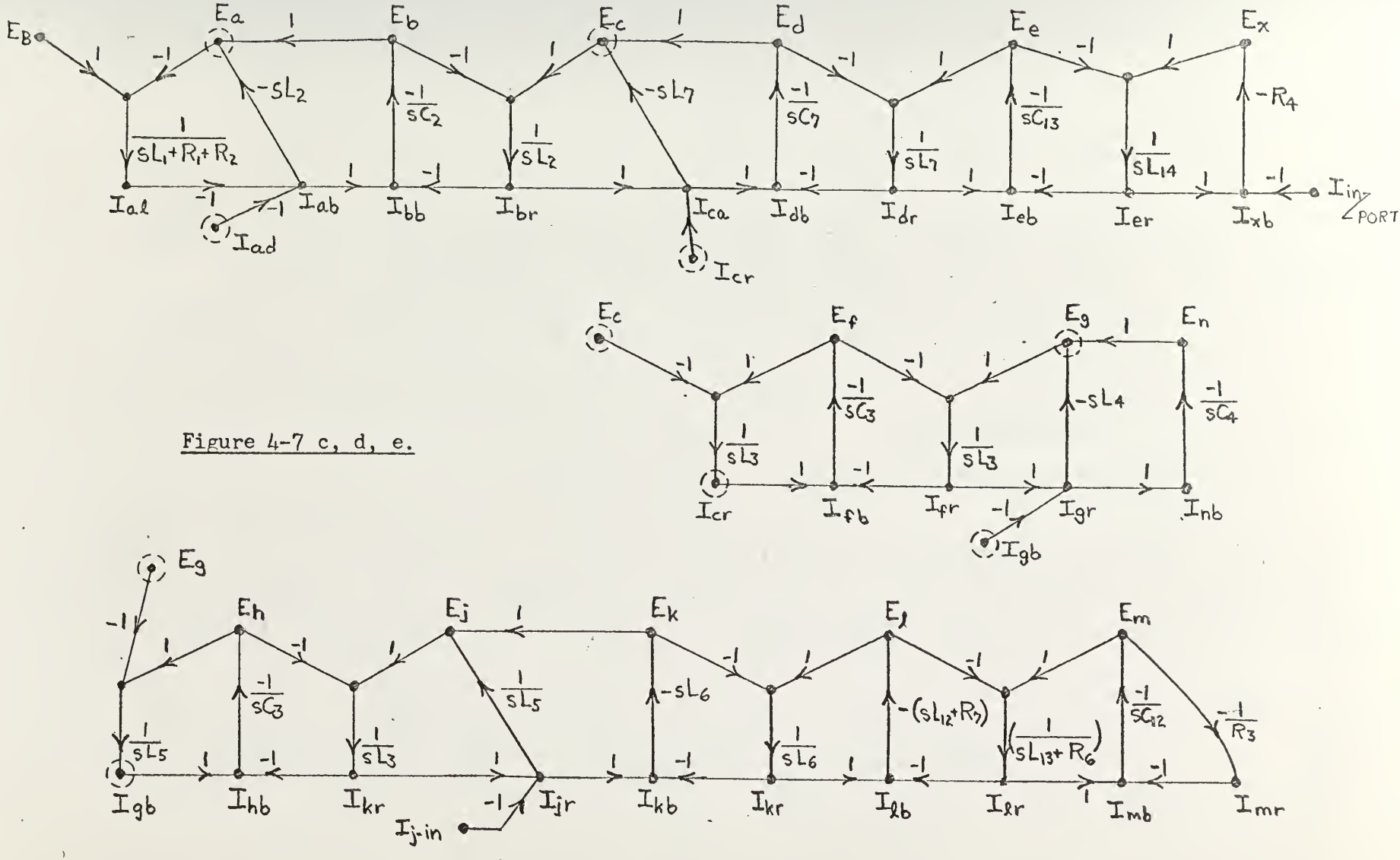

Figure 4-7 c, d, e.

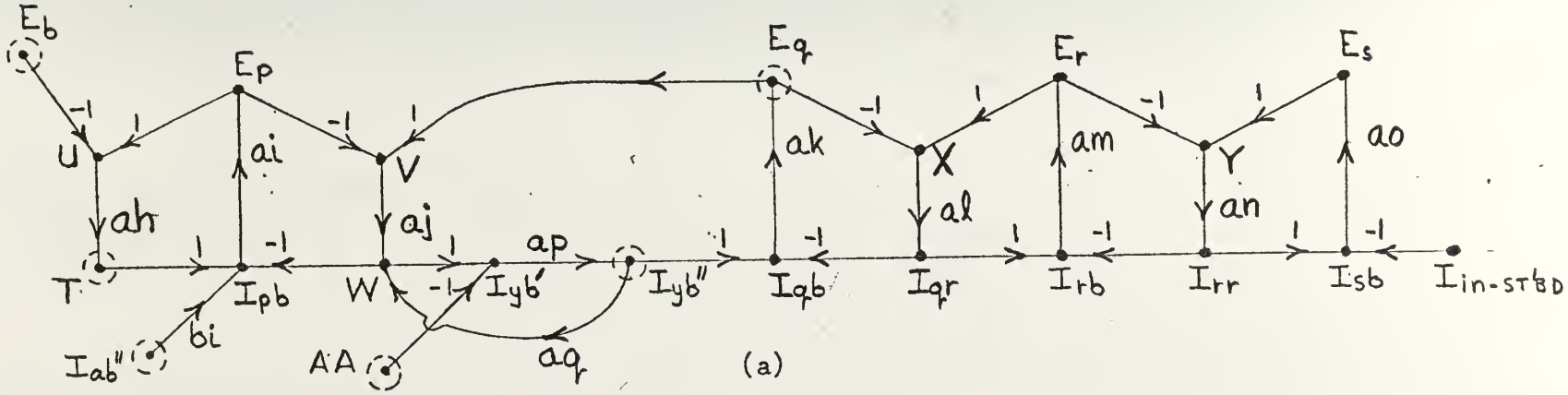

Figure 4-8 a, b.

Final Flow Graph of d-c System

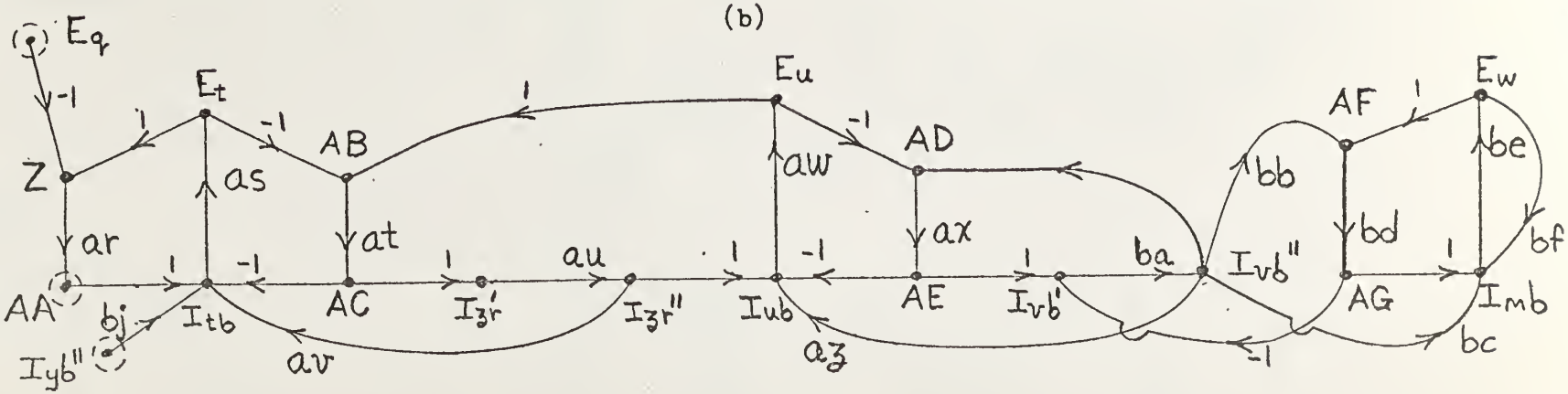

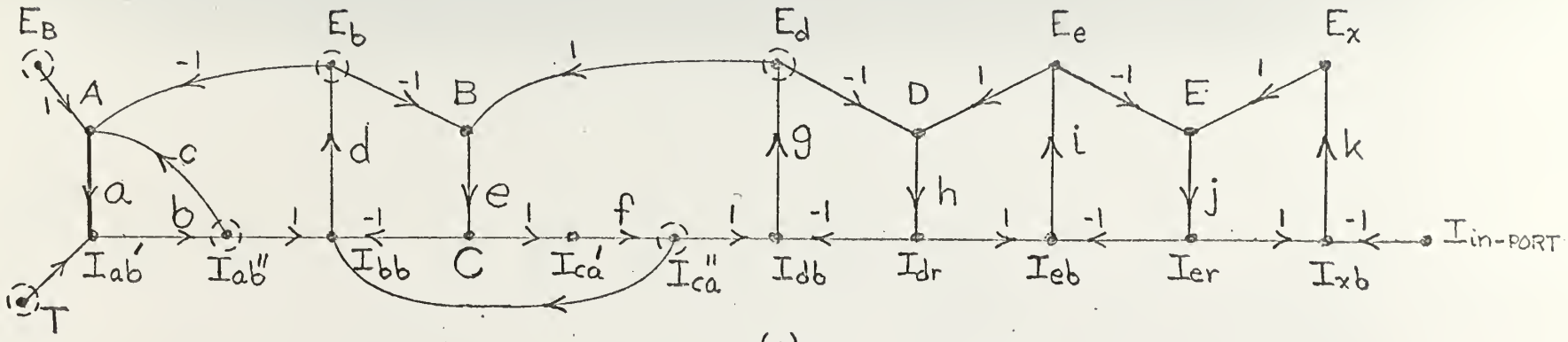

(c)

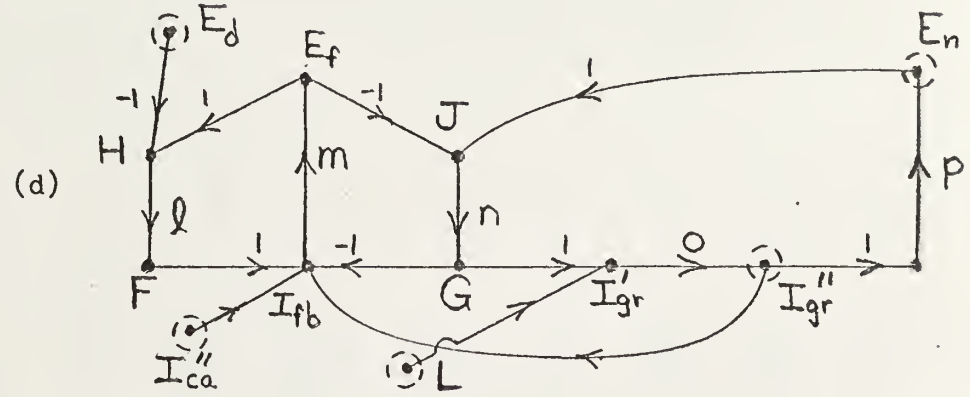

(d)

Figure 4-8 c, d, e.

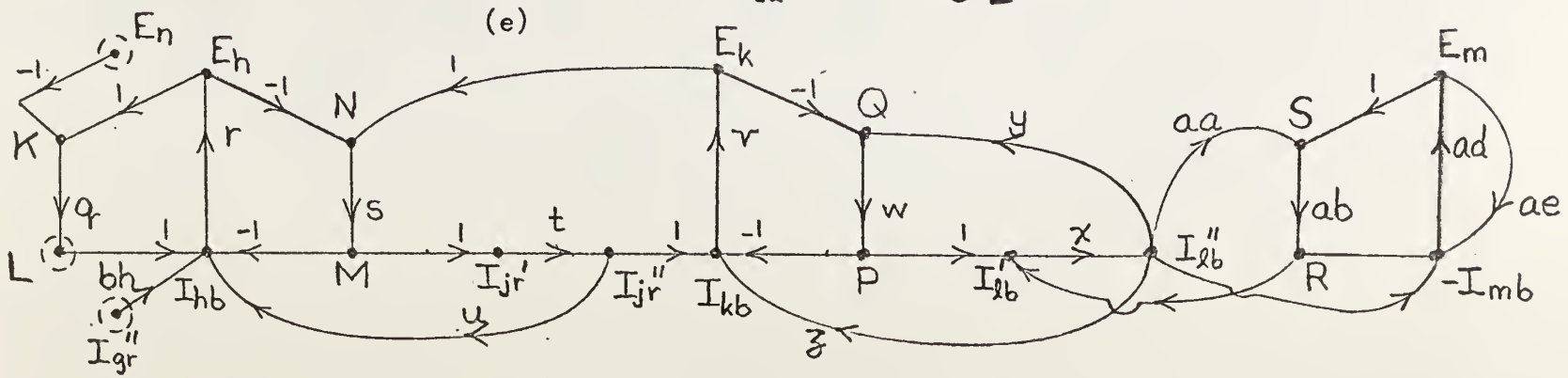

(e)

Table 4-1

Transmissions of Final Flow Graph

$$a = \frac{-1}{sL_1+R_1+R_2} \qquad p = \frac{-1}{sC_4}$$

$$b = \frac{1}{1+\frac{L_2}{L_1}+\frac{L_2}{L_8}} \qquad q = \frac{1}{sL_5}$$

$$c = \frac{-L_2(R_1+R_2)}{L_1} \qquad r = \frac{-1}{sC_5}$$

$$d = \frac{-1}{sC_2} \qquad s = \frac{1}{sL_5}$$

$$e = \frac{1}{sL_2} \qquad t = \frac{1}{1+\frac{L_6}{L_5}}$$

$$f = \frac{1}{1+\frac{L_7}{L_2}+\frac{L_7}{L_3}} \qquad u = \frac{L_6}{L_5}$$

$$g = \frac{-1}{sC_7} \qquad v = \frac{-1}{sC_6}$$

$$h = \frac{1}{sL_7} \qquad w = \frac{1}{sL_6}$$

$$i = \frac{-1}{sC_{13}} \qquad x = \overline{1+}$$

$$j = \frac{1}{sL_{14}} \qquad y = -R_7$$

$$k = -R_4 \qquad z = \frac{L_{12}}{L_6}$$

$$l = \frac{1}{sL_3} \qquad aa = R_7 - R_6\frac{L_{12}}{L_{13}}$$

$$m = \frac{-1}{sC_3} \qquad ab = \frac{1}{sL_{13}+R_6}$$

$$n = \frac{1}{sL_3} \qquad ac = \frac{L_{12}}{L_{13}}$$

$$o = \frac{1}{1+\frac{L_4}{L_3}+\frac{L_4}{L_5}} \qquad ad = \frac{-1}{sC_{12}}$$

$$ae = \frac{1}{R_3}$$

$$af = \frac{L_2}{L_7}$$

$$ag = \frac{L_4}{L_3}$$

$$ah = \frac{1}{sL_8}$$

$$ai = \frac{-1}{sC_8}$$

$$aj = \frac{1}{sL_8}$$

$$ak = \frac{-1}{sC_9}$$

$$al = \frac{1}{sL_9}$$

$$am = \frac{-1}{sC_{13}}$$

$$an = \frac{1}{sL_{15}}$$

$$ao = -R_5$$

$$ap = \frac{1}{1 + \frac{L_9}{L_{10}} + \frac{L_9}{L_8}}$$

$$aq = \frac{L_9}{L_8}$$

$$ar = \frac{1}{sL_{10}}$$

$$as = \frac{-1}{sC_{10}}$$

$$at = \frac{1}{sL_{10}}$$

$$au = \frac{1}{1 + \frac{L_{11}}{L_{10}}}$$

$$av = \frac{L_{11}}{L_{10}}$$

$$aw = \frac{-1}{sC_{11}}$$

$$ax = \frac{1}{sL_{11}}$$

$$ay = -R_7$$

$$az = \frac{L_{12}}{L_{11}}$$

$$ba = \frac{1}{1 + \frac{L_{12}}{L_{11}}}$$

$$bb = R_7 - R_6\frac{L_{12}}{L_{13}}$$

$$bc = \frac{L_{12}}{L_{13}}$$

$$bd = \frac{1}{sL_{13} + R_6}$$

$$be = \frac{-1}{sC_{12}}$$

$$bf = \frac{1}{R_3}$$

$$bg = \frac{L_7}{L_3}$$

$$bh = \frac{L_4}{L_5}$$

$$bi = \frac{L_2}{L_8}$$

$$bj = \frac{L_9}{L_{10}}$$

Table 4-2

Initial conditions

Flow graph nodes and corresponding circuit variables at $t = 0$.

Node	Circuit Variables
I_{ab}'	$-(i_{al} \cdot L_1 + i_{ab} \cdot L_2)/L_1$
E_b	e_b
C	$(i_{br} \cdot L_2 + i_{ca} \cdot L_7)/L_2$
E_d	e_d
I_{dr}	i_{dr}
E_e	e_e
Ier	i_{er}
F	$(i_{cr} \cdot L_3 - i_{ca} \cdot L_7)/L_3$
E_f	e_f
G	$i_{qr} + i_{gr}$
E_n	e_n
L	$(i_{gb} \cdot L_5 - i_{gr} \cdot L_4)/L_5$
E_k	e_k
M	$(i_{kr} \cdot L_5 + i_{jr} L_6)/L_5$
E_h	e_h
P	$(i_{kr} L_6 + i_{lb} L_{12})/L_6$
R	$(i_{lr} L_{13} - i_{lb} L_{12})/L_{13}$
E_m	e_m

T	$(i_{aa} \cdot L_8 - i_{ab} \cdot L_2) / L_8$
E_p	e_p
W	$(i_{pr} \cdot L_8 + i_{yb} \cdot L_9) / L_8$
E_q	e_q
I_{qr}	i_{qr}
E_r	e_r
I_{rr}	i_{rr}
AA	$(i_{yr} \cdot L_{10} - i_{yb} \cdot L_9) / L_{10}$
E_t	e_t
AC	$(i_{tr} \cdot L_{10} + i_{gr} \cdot L_{11}) / L_{10}$
E_u	e_u
AE	$(i_{ur} L_{11} + i_{vb} L_{12}) / L_{11}$
AG	$(i_{vr} L_{13} - i_{vb} L_{12}) / L_{13}$

Table 4-3

Circuit Values
(Refer to Fig. 4-1)

Component Number	Inductance (microhenrys)	Capacitance (microfarads)	Resistance (ohms)
1	975.		.0054
2	8.10521	.05981	0
3	11.3793	.09464	.594
4	4.1518	.032114	.000 796*
5	1.3987	.005358	.000 796*
6	1.01399	.004 414	.0175
7	6.4795	.0477	61.7
8	6.9658	.05273	
9.	6.7083	.04894	
10	3.8406	.017279	
11	.64076	.002411	
12	49.4 henrys	5.65 farads	
13	614.	.0104	
14	140.		
15	140.		

* This value is for the two diodes in their conducting state; in the blocking state, they would be 4,260 ohms.

5. System Simulation.

5.1 Analog and Digital Computers as Simulation Devices.

5.1.1 General.

One of the requirements imposed upon the mathematical model in the previous section was that it be amenable to system simulation by computer, either analog or digital. This requirement has been met with the signal flow graph. Each transmission of the flow graph, Fig. 4-8, is of a form readily programmed on an electronic analog computer; similarly, each node is either a summing junction or signal distribution point, which may also be readily programmed. With regard to digital computer simulation, routines are available for the solution of a set of simultaneous linear differential equations; such equations are readily formulated in the proper format from the flow graph. The choice of vehicle for the simulation then is based upon the relative advantages/disadvantages of the computers available with respect to the system to be simulated.

5.1.2 Electronic Analog Computer.

The advantages of simulation by analog computer are as follows:

a. The effect of varying system parameters, initial conditions, and independent forcing functions is immediately observable at the output terminals of the operational amplifiers.

b. The system can be readily expanded or reduced with little effect on the overall program.

c. The continuous and instantaneous character of analog computer transmissions obviates the necessity of removing gain loops from the flow graph.

On the other hand certain disadvantages which occur with analog simulation are discussed in the following paragraphs.

The useful linear range of operational amplifiers is limited. The lower limit is a function of the internal noise of the amplifier, and for those variables being recorded, it is also a function of the sensitivity of the recording instrument; at the upper limit, saturation occurs. For all but a very simple system, these limitations generally necessitate scaling the variables such that their voltage analogs always remain within the linear range of the amplifier. Additionally, it is often desirable to scale the independent variable, herein considered to be time, in order to extend the observation interval for short duration effects, or to compress the interval of long term responses. The degree of difficulty of proper scaling increases in proportion to the increasing order of the system to be simulated.

In removing the several differentiating transmission that occurred in the basic flow graph, a number of the system's impedance parameters lost their separate identity as coefficients. Each of these parameters was caused to appear in two or more new coefficients in different combinations with other parameters. On analog computers, the significant figures of the coefficients are normally set as fractions on potentiometers; their order of magnitude is programed using the gain, or attenuation, associated with the input and feedback impedances of the amplifiers. The accuracy to which the potentiometers may be set is generally limited to four significant figures, and is usually less. Unless each parameter is consistently represented in each of the several coefficients where it appears, the characteristic roots of the system may be shifted sufficiently to appreciably alter the system's response. In fact, for a system which has roots with small, negative, real parts, small inconsistencies in the several coefficients may be sufficient to drive the real part of these roots positive, resulting in

an apparently unstable system, truly an anomaly when the system is a passive electrical network. This difficulty can only be minimized by retaining a sufficient number of figures of each parameter-factor of the coefficients to insure against error in the fourth significant figure of the coefficients themselves.

The passive parameters of the circuit model established in this study are considered constant throughout the duration of the transient; however, more complete data concerning resistance vs. load characteristics of the silicon-controlled rectifier, and knowledge of the exact configuration of the power supply circuitry may lead to a model of this device in which the resistance is both time and load variant. Considerable expertise may be required to accurately program these non-linearities on the analog computer.

The number of operational amplifiers required for large system simulation may be prohibitive. Consider the solution by repeated integration of the n-th order differential equation shown below in Laplace transform notation:

$$\frac{C}{R} = \frac{\sum_{i=0}^{n-1} a_i s^i}{\sum_{j=0}^{n} b_j s^j} \qquad (5\text{-}1)$$

Now, let

$$W = \frac{R}{\sum_{j=0}^{n} b_j s^j} \qquad (5\text{-}2)$$

Then,

$$C = W \sum_{i=0}^{n-1} a_i s^i \qquad (5\text{-}3)$$

Equation (5-3) is illustrated by the flow graph, Fig. 5-1.

Thus the solution can be obtained by n successive integrations. In addition to the n amplifiers required for the integrations, a sign inversion

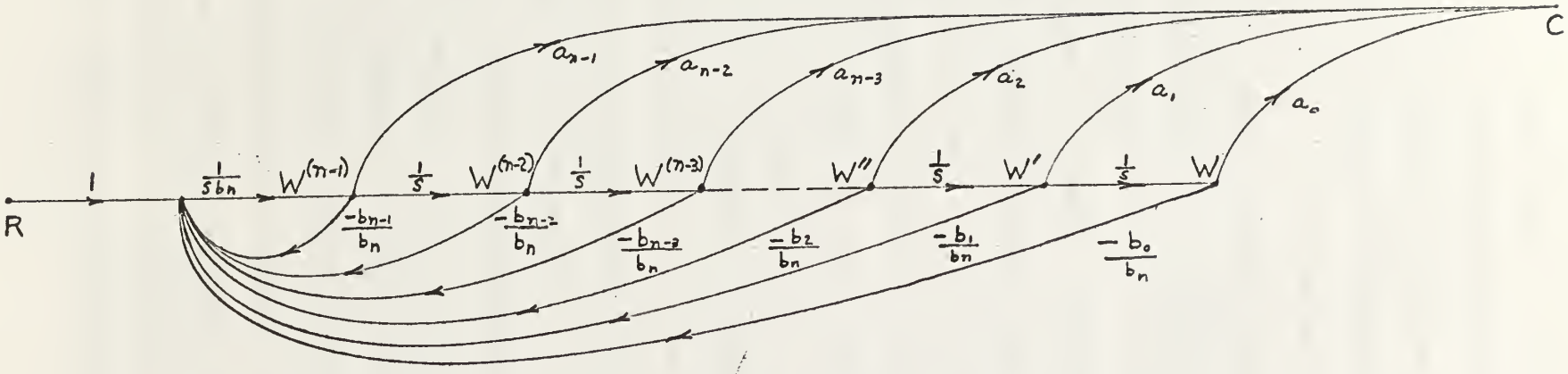

Figure 5-1
Solution of n-th Order
Differential Equation

must be effected after every alternate integration to provide the proper signs of the feed-back and the feed-forward transmissions. These inversions may be accomplished by a single amplifier for each direction. The minimum number of amplifiers required is therefore $n+2$, in addition to those that may be required to establish the proper magnitude of coefficients. The circuit shown in Fig. 4-1 is a thirty-second order system; based upon the preceeding discussion at least thirty-four amplifiers would be required to provide a solution to the differential equation relating an input-output pair. Considering the flow graph, Fig. 4-8, as a basis for simulation, the number of amplifiers required is expanded considerably. Each of the closed loops that form the main lattice of the flow graph provide negative feedback to all nodes touching the loop. There are, however, two integrators per loop and to provide negative feedback on an analog computer requires an odd number of amplifiers between an input quantity and the feedback. Thus each loop requires an inverting amplifier in addition to those required for integration. By placing the inverters in branches common to two loops, the number of these inverting amplifiers required is minimized. With such an arrangement, certain of the voltages and currents will be of opposite polarity from that shown on the flow graph, but this is of small concern. There are, in addition to the loops making up the lattice, nineteen other transmissions which will require a sign inversion in an analog simulation. The number of amplifiers required for system simulation, preserving as accessible nodes all circuit node voltages and branch currents shown in Fig. 4-8, is then 3/2 the number of integrators plus 19, i.e., 67. As with the solution of the differential equation, this number does not include amplifiers required solely to establish the proper magnitude of coefficients. The maximum number of amplifiers available at the time of

this study was 60, and this lack of sufficient amplifiers precluded using the analog computer for a full system simulation. Where sufficient amplifiers are available, or when lower ordered systems are studied, its other limitations notwithstanding, an analog simulation would be of considerable value in a study of this type.

5.1.3 Digital Computer.

The discussion which follows is based upon the use of Fortran language with a large, general purpose computer, specifically the Control Data Corporation 1604 Computer.

The advantages of a digital computer simulation are:

a. System changes are readily programmed from the modified signal flow graph.

b. No scaling is required. Quantities varying over many orders of magnitude are readily accommodated.

c. The different time frames for the various time duration effects may be stipulated in the same program, subject to limitations described below.

d. The impedance parameters - inductance, capacitance, and resistance - need be specified only once; they will be retained in memory within the computer with an accuracy of eight significant figures. Thereafter, all computations involving these parameters will be executed using consistent values of the entering arguments, and the accuracy with which the computer coefficients will be used far exceeds that attainable with the analog computer.

e. Programs for the simulation of systems of high order can be handled within the large memory of the computer.

f. System non-linearities can be programmed to whatever degree of accuracy may be desired.

g. Recorded results may include tabulated as well as graphical data.

There are corresponding limitations of the digital computer which are discussed in the following paragraphs.

The solution of the system's differential equations is accomplished by numerical integration. The largest time increment consistent with an accurate solution is generally considered to be 1/100 of the period of the fastest oscillation. If sustained high-frequency oscillations are super-imposed upon lower frequency oscillations, or upon long time-constant damping, many hours of computer time may be required to generate a steady-state solution. If, on the other hand, the damping ratio of the high frequency waves is relatively large, they will be attenuated after a few cycles and a larger integration time increment can then be used. Unless the approximate locations of the system's roots are known, several computer runs may be required to determine the sequence of time steps and the proper time to introduce each in order to generate the steady state solution in minimum computer time.

The iterative nature of the digital computer solution forms the basis of the problem of pure gain loops which was mentioned in Section 4. Consider the transmission from w to z shown in Fig. 5-2.

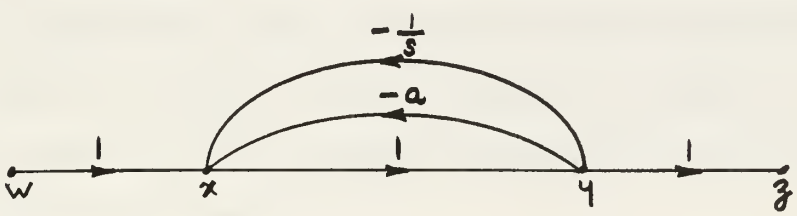

Figure 5-2
Pure Gain Loop

Algebraically,

$$x = w - a y - \int y \, dt \tag{5-4}$$

$$y = x \tag{5-5}$$

$$z = y \tag{5-6}$$

A simultaneous solution of these three equations, for $w(t) = 1 u(t)$ yields the following:

$$z(t) = e^{-\frac{1}{1+a}t} \tag{5-7}$$

Now, consider the solution of the system by numerical integration for Δt very small, and $a \gg 1$. Table 5-1 shows the values of the various variables at time zero, and after each of the first three time increments. Where used, ε represents a value very small compared with the other quantities with which it is summed.

t	w	x	y	z
0	1	1	1	1
1	1	$1 - a - \varepsilon$	$1 - a - \varepsilon$	$1 - a - \varepsilon$
2	1	$1 - a + a^2 - \varepsilon$	$1 - a + a^2 - \varepsilon$	$1 - a + a^2 - \varepsilon$
3	1	$1 - a + a^2 - a^3 - \varepsilon$	$1 - a + a^2 - a^3 - \varepsilon$	$1 - a + a^2 - a^3 - \varepsilon$

Table 5-1

Thus, when a is large, the highest power term dominates, and the output increases in magnitude at each iteration by a factor approximately equal to a , and it alternates in sign. Ignoring the feedback effect of the integration path, it can be seen that the values of the output represent, in part, the series expansion

$$\frac{1}{1+a} = 1 - a + a^2 - a^3 + \cdots + (-1)^{n-1}a^n + (-1)^n a^{n+1} + \cdots + (-1)^{r-1}\frac{a^r}{1+a} \qquad (5\text{-}8)$$

When $a<1$, the series can be terminated after n terms with an error less than the magnitude of the $(n+1)$ th term [13]. For $a>1$, however, the series must always include the remainder term, the r-th term of equation (5-8). The error introduced by omitting the remainder is seen to increase without bound as the series is expanded. When a rectangular integration scheme is employed, the series will expand by one term for each time increment; for more accurate numerical integration processes, such as the fourth order Runge-Kutta method [10, 18], the system Fortran equations may be executed by the computer more than once for each Δt, causing an even more rapid expansion of the series. The two techniques which, in general, provide more accurate numerical solutions to differential equations - smaller increments of the independent variable, and refined estimates of the slope between steps - will, for the case of the gain loops, cause a more rapid divergence of the error. The problem can be eliminated by absorbing one of the nodes and transforming the loop into a node-to-node transmission as discussed in Section 4.3.4 and illustrated in Fig. 4-6.

A further drawback of digital computers as simulation devices is the fact that the effects of parameter variation are not readily apparent. The extent to which the effects may be observed depends upon factors not directly associated with the problem to be solved. Two such factors are the accessibility of the computer to the engineer, and the type of on-line display equipment available with the computer.

5.1.4 Other Simulation Schemes.

Investigation of other simulation schemes was limited by the time available for the study. One simulation method worthy of consideration for any future study is the use of a digital analog, (hybrid) computing scheme, by which it may be possible to select the advantages of both computers and to minimize their disadvantages.

5.2 Digital Computer Program.

The flow graph, Fig. 4-8, shows the system to be described by an inter-connected network of transfer functions. Everywhere it appears, the Laplace transform variable, s, is in the denominator and is of first degree. Thus,

$$\frac{X_{out}}{X_{in}} = \frac{K}{s+P}$$

By cross-multiplying and rearranging terms we obtain

$$sX_{out} = K X_{in} - P X_{out}$$

and inverting this to the time domain yields the first order differential equation:

$$\frac{d(X_{out})}{dt} = K X_{in} - P X_{out}$$

Thirty two such equations were formulated from the system flow graph. These and the equations describing the inter-connections were used with a computer library routine, Subroutine INTEG 1 [18] to provide a numerical solution to the thirty-second order system.

5.3 Simulation Problems.

The first attempts at simulation were made using only a small section of the distribution system. It was with this small section that the problem of simulating gain loops, described in Section 5.1.3, was encountered. Even in the small network chosen, the cause of the rapid divergence was not

readily apparent. The network chosen for the trial simulation was the circuit model of the drain pump. This network forms a part of the illustrative circuit, Fig. 4-2; its flow graph, after the removal of the differentiating transmission, is shown in Fig. 5-3. The forcing function is a current into the circuit node ℓ from some other part of the system. The

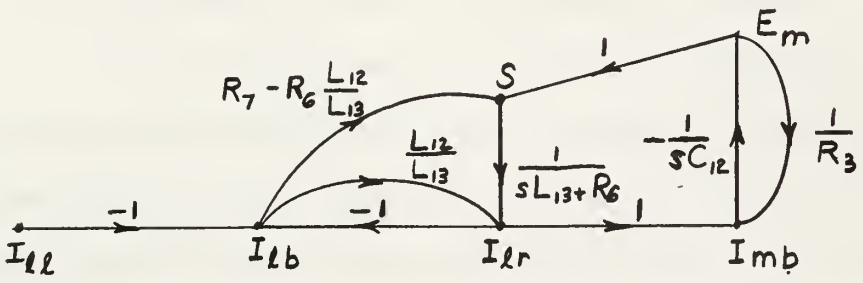

Figure 5-3
Signal Flow Graph of Drain Pump

closed gain loop, $-\frac{L_{12}}{L_{13}}$ touches nodes $I_{\ell b}$ and $I_{\ell r}$. Gain transmissions connect these nodes with nodes S and I_{mb} respectively. Thus the divergence caused by the gain loop has almost instantaneous effect not only upon the nodes which touch it but also upon any node having an input signal which is a gain-only function of the nodes touching this loop. In the test circuit then, four of the six nodes were rapidly divergent. Recognition of the problem's cause occurred only when the values of all the variables were printed after each execution of the equations by the computer.

5.3.2 Transmission Gains.

The problem of accuracy in potentiometer settings for gains and other coefficients, when such values were computed values involving more than a single parameter, was described in Section 5.1.2. When "slide rule accuracy" values were used as input data for the digital computer, an instability

occurred there also. When the values of the parameters themselves were used as input data and all coefficients and transmissions computed within the program, the results indicated a stable system which agreed with the analytical solution.

5.3.3. Time Increments.

As stated in Section 3., the lumped circuit equivalent model of the transmission line was developed for a best frequency match of 0.1 mc. It was expected that this would be close to the dominant frequency of the system. However, for all simulations of parts of the system which included one or more of the transmission line T-sections, the model was found to be unstable for integration step sizes greater than 0.01 microseconds. Many times the instability caused by too large a time step was not apparent until the program had progressed through a large number of iterations. Low frequency oscillations, of initially large magnitude, would be damped but then the high frequency perturbations would become relevant and eventually cause exponential growth. Without a complete determination of the system's characteristic equations, it is not possible to more precisely predict the dominant frequencies.

6. Results and Conclusions.

6.1 Results.

A method for developing a system model and for simulating that model on a digital computer was developed and is shown. The simulation program was not perfected, and never ran correctly for the entire system. The time increment needed to keep the numerical integrations from diverging was very small; the computer program was running two hours in order to simulate fifty three microseconds.

The method of development is believed to be good, and future studies should benefit from it. The incompatibility of gain loops and numerical integration methods is a fact that should be known before digital computer simulation is started.

6.2 Conclusions.

6.2.1. Routines for the solution of systems of differential equations, such as INTEG 1, are useful tools for simulation.

6.2.2. A valid way to test the simulation of the system or its components is by allowing it to change from some known initial state to another, known, final state; to either start with zero current and voltage and to "close the switch on the battery" or start with energy stored in the system and allow it to be dissipated. The flexibility of the digital computer allows a single branch or the entire network to be tested in this manner with only slight changes in the program.

This check-out technique was time consuming, however. A preliminary, much shorter method of indicating convergence, was to put the expected final values in the program as initial conditions and see if they were stable.

6.2.3 Although it was plausible to call the transmission lines lossless, including a slight resistance in the model for them would have been a good idea. If nothing else, computation time would be decreased because of the smaller transient decay times.

APPENDIX A

Bibliography

1. Stephen S. ATWOOD, Electric and Magnetic Fields, John Wiley & Sons, Inc., 1932.

2. Bureau of Ships letter Serial: 660D-456, of 10 Feb. 1965.

3. Bureau of Ships drawing SSN588-345-1854682-H, Emergency Propulsion and DC Power Distribution Diagram.

4. Bureau of Ships drawing SSN588-345-1854683-H; Emergency Propulsion & DC Power Wiring Deck Plan.

5. J. L. FINK, J. F. JOHNSTON, F. C. KRINGS, The Application of Static Inverters for Essential Loads. IEEE Transactions on Power Apparatus and Systems, v. 82, Dec. 1963, 1068-72.

6. General Electric, General Engineering Laboratory Report No. 62GL174, Analog Study of Naval Shipboard Power System, Dec. 28, 1962, by LEIBY and WINKELJOHANN.

7. General Electric, General Engineering Laboratory Confidential Report No. 62GL77, S5G Power Supply Development, May 25, 1962, by D. P. SHATTUCK, W. McMURRAY, F. G. TURNBULL.

8. B. HAGUE, The Principles of Electromagnetism Applied to Electrical Machines. Dover Publications, Inc., 1962.

9. E. K. HOWELL, Protecting SCR's and Silicon Rectifiers, Control Engineering, v. 10, Dec. 1963. 63-67.

10. W. JENNINGS, First Course in Numerical Methods, McMillan Co., N. Y., 1964.

11. W. KAPLAN, Advanced Calculus, Addison-Wesley Co., Massachusetts, 1959.

12. E. W. KIMBARK, Electrical Transmission of Power and Signals. John Wiley & Sons, Inc., N. Y., 1949.

13. S. J. MASON and H. J. ZIMMERMAN, Electronic Circuits, Signal and Systems, John Wiley & Sons, Inc., N. Y., 1960.

14. Naval Research Laboratory, NRL Report 3707, Transient Electrical Characteristics of Lead-Acid Submarine Batteries, 30 June 1950, by B. G. BINGHAM.

15. Naval Research Laboratory, NRL Report 3839, Impedance Measurements of a Lead-Acid Storage Battery Cell, 27 July 1951, by J. H. KLUCH.

16. F. E. TERMAN, Electronic and Radio Engineering, McGraw-Hill, 1955.

17. G. W. VINAL, Storage Batteries, John Wiley & Sons, Inc., 1955.

18. J. R. WARD, Numerical Solution of Ordinary Differential Equations, CO-OP ID: D2-NPS-INTEG1, U. S. Naval Postgraduate School Computer Center, June 1964.

19. E. WILLIHNGANZ, P. ROHNER, Battery Impedance: Farads, Milliohms, Microhenrys, Proceedings AIEE, Sept. 1959, 259-262.

APPENDIX B

DISTRIBUTED PARAMETERS of CABLING

B.1 Inductance.

B.1.1 Special Considerations.

Although numerous reference works on transmission line theory are available, two geometrical factors of the submarine d-c distribution system require special attention in the development of the distributed inductance relationships: (1) the location of the multi-cable system close to the high permeability steel hull, resulting in fields which vary azimuthally as well as radially; (2) the proximity effect - when the distance of separation of adjacent cables is not large relative to the linear cross-section dimension, the adjacent sides of the cables will be linked by more flux than will the far sides.

B.1.2. Method of Images.

Consider the magnetic field established by a long, straight, cylindrical, current-carrying conductor located in a region of low magnetic permeability and far removed from other conductors and from any region of higher permeability. The constant flux lines of the magnetic field in the region are a series of circles concentric with the axis of the conductor. If the conductor is now brought to the vicinity of other conductors, and near a boundary separating the low permeability (air) region from one of high permeability (steel), the flux lines are no longer symmetric in azimuth about the center of the conductor; the total flux distribution is influenced by the relative polarities and the magnitudes of all the currents, and by the shape and proximity of the air-steel boundary. For the case where all the currents are parallel to a plane, vertical

boundary,[1] the boundary conditions of the horizontal and tangential components of the magnetic flux lines on the air side of the boundary are identically satisfied as follows:[2]

a. For each actual conductor postulate an image conductor located on the opposite side of the boundary, and at equal distance from the boundary as the actual conductor, i.e., at the image point of the original conductor.

b. Establish in each image conductor a current equal to that in the corresponding actual conductor, multiplied by a factor of

$$K_\mu = \frac{\mu_s - \mu_a}{\mu_s + \mu_a} \qquad \text{(B-1)}$$

where μ_s and μ_a are respectively the permeabilities of the steel and air.

c. Consider the region surrounding the conductors, both actual and image, to have permeability μ_a.

Thus, the problem of determining the strength of a single, highly asymmetric field reduces to the relatively straightforward superposition of $2n$ symmetric fields, where n is the number of actual conductors. When the permeability of the second medium is very much greater than that of the first, as is the case with steel and air, K_μ approaches unity, and both actual and image currents may then be considered equal.

[1] The submarine hull is actually not a plane surface at any point, but rather is circular in corss-section. However, its center of curvature is sufficiently far from the centers of the cables that it may be regarded as a plane for the purposes of this discussion.

[2] No attempt is made herein to justify the method of images as it is applied to magnetic fields. For the theory of magnetic images see [1] and [8] .

A typical configuration of submarine d-c power cables and steel hull boundary is shown in Fig. B-1a. The equivalent system, from an inductance point of view, with image conductors added and steel hull removed, is shown in Fig. B-1b. All subsequent calculations for the distributed inductance are based upon the model of Fig. B-1b, which may be modified to include more, or fewer cables, and different relative locations of the opposite polarities.

B.1.3. Flux Linkages. The magnetic flux linkage of each conductor is the sum of:

a. Self-linkage of a current by the flux established by that current

(1) Partial flux linkages by lines of flux within the conductor;

(2) Total linkage by all lines outside the conductor;

b. Mutual-linkage of each current with flux established by the current of each other conductor (See Fig. B-2).

(1) Partial linkage of current in conductor 1 by flux of current in conductor 2 at distance ρ from the center of conductor 2, where

$$D - r_c < \rho < D + r_c$$

(2) Total linkage of all current in conductor 1 by the flux of conductor 2 when $\rho \geq D + r_c$.

The flux linkages of a.(1) and b.(1) above will be modified by the "skin effect" of high frequencies. In the self-linkage term, this effect will be taken into account by adjusting the computed d-c value according to tabulated ratios. For the mutual flux linkage term, the skin effect is

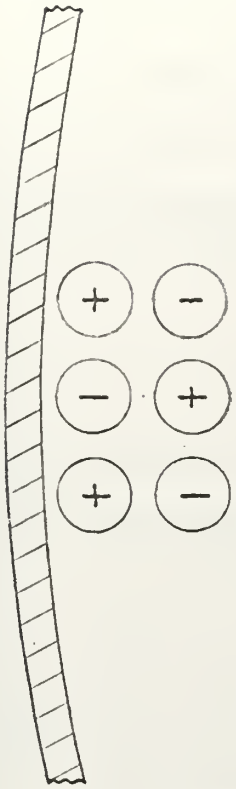

Figure B-1a

Typical d-c cable configuration for hull mounted power cables.

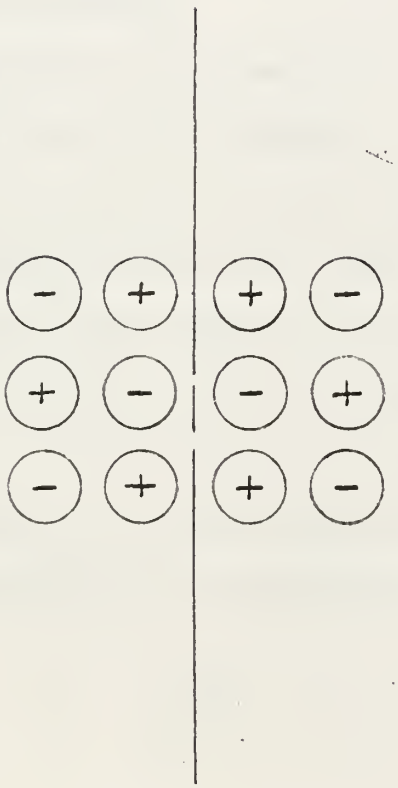

Figure B-1b

Image model of Fig. B-1a. Hull has been removed and image conductors added. Note: the image conductor has the same polarity as the corresponding actual conductor.

integrally treated in the general development of the appropriate formula.

B.1.4. Internal Self-linkage. The basic d-c relationship and the skin effect receive considerable attention in transmission line reference works; consequently only the necessary results are presented herein. For the d-c case

$$\lambda_{ii(\text{internal})} = \frac{\mu I_i}{8\pi} \quad \text{webers/meter} \qquad \text{(B-2)}$$

For skin effect calculations, a table of internal self-inductance ratios is available [12] ; the entering argument for the table is the quantity

$$x = r_c \sqrt{\frac{\omega \mu}{\rho}} \qquad \text{(B-3)}$$

where r_c is the radius of the conductor,

ω is the radian frequency,

μ is the permeability of the conductor,

and ρ is the resistivity of the conductor.

The table may be used for values of $x \leq 100$. Where x falls between two values for which the inductance ratios are listed, linear interpolation between the two given values will yield results to a sufficient degree of accuracy for most calculations. It is of interest to note the wide variation of the ratio:

at $x = 0$, $L_{ac}/L_{dc} = 1.000$; at $x = 100$, $L_{ac}/L_{dc} = 0.028$. For values of $x > 100$, a close approximation to the inductance ratio is given by

$$\frac{L_{ac}}{L_{dc}} = \frac{2\sqrt{2}}{x} \qquad \text{(B-4)}$$

B.1.5. External Self-linkage. The desired effect of introducing image currents was to obtain azimuthal symmetry of the flux field of each conductor considered separately. The contribution to external linkage of each conductor by its own current, when such symmetry is established, is given by the expression

$$\lambda_{ii(external)} = 2 \times 10^{-7} \ln 1/r_c \text{ webers/meter} \quad \text{(B-5)}$$

It is important to note at this point that the above relationship can be derived only when all conducting paths, forward and return, of the transmission circuit are considered. Any development of inductance or flux linkage relationships, for flux external to a conductor, will result in an indeterminate mathematical expression if the complete circuit is not considered. For example, the analytical expression for the external self-inductance of a single conductor, without reference to any other conductor, is

$$L_i(\text{external}) = 2 \times 10^{-7} \ln r \Big]_{r = r_c}^{r \to \infty} \text{ henrys/meter} \quad \text{(B-6)}$$

B.1.6. Partial Mutual Linkages. The necessity of considering the proximity effect is generally obviated by assuming that the center-to-center separation of the conductors is much greater than the radius of the conductor. In the submarine d-c distribution system, such an assumption is unwarranted; the separation of the cables is generally of the order of only 2 - 3 times the conductor radius. A general development is pursued wherein the conductor area of the cable is an annular ring of outside radius r_c and inside radius r_δ . (Fig. B-2). Radius r_δ is a function of frequency and at d-c becomes zero; at high frequencies it is approximated by the difference between the conductor radius r_c and the skin

Typical geometry of internal mutual flux linkage,
illustrating the parameters of proximity and skin effects.

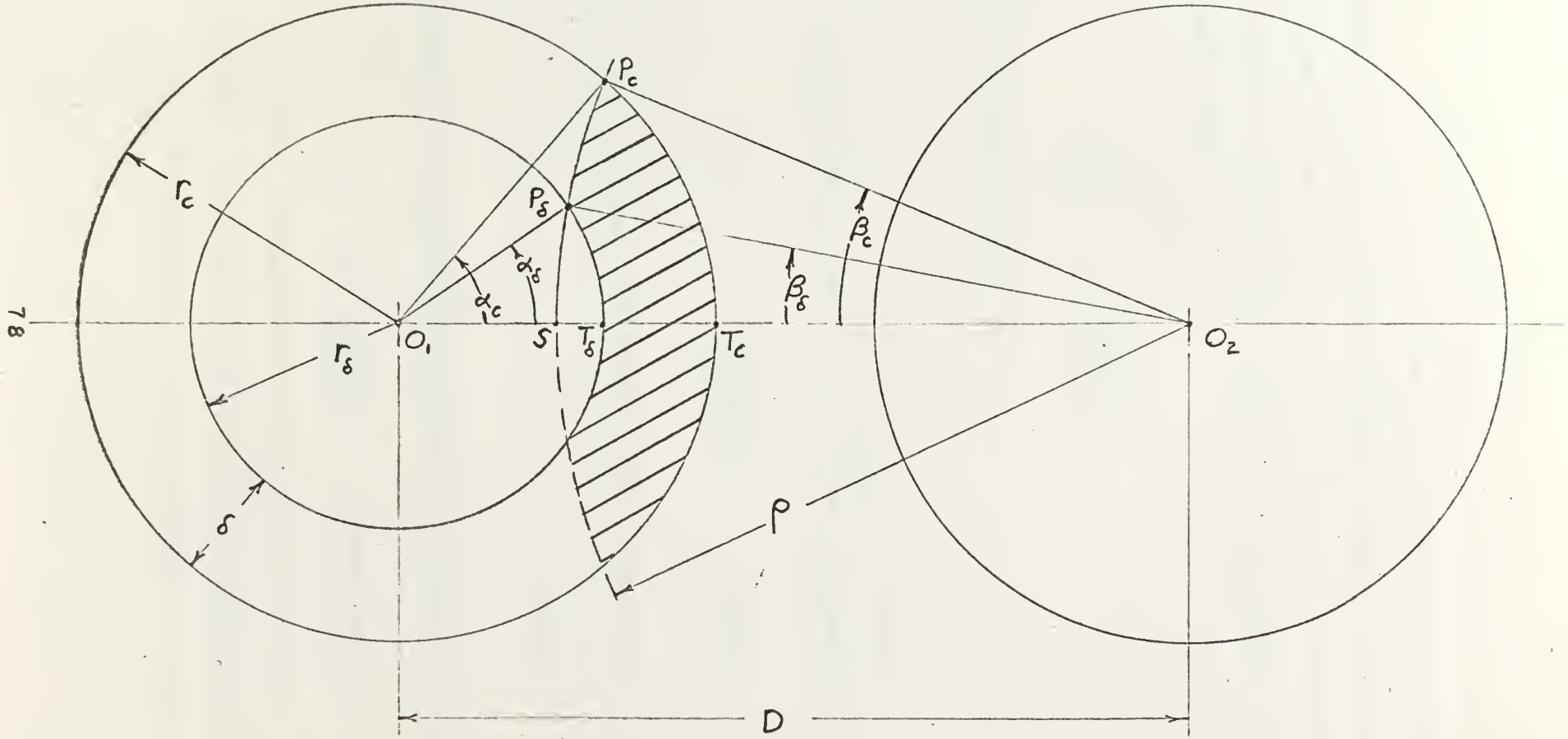

Figure B-2

penetration depth δ . As frequency is decreased however, the error of this approximation becomes very large. For the same entering argument x that was used with the internal self-inductance skin effect corrections, tabulations of a-c/d-c resistance ratios for solid, round wires are available. Now, if the resistance is considered to be constant across the annular conduction area, and the resistivity of the conductor invariant with frequency, then

$$\frac{R_{ac}}{R_{dc}} = \frac{\pi (r_c^2 - r_\delta^2)}{\pi r_c^2} \qquad \text{(B-7)}$$

Solving equation (B-7) for r_δ

$$r_\delta = r\sqrt{1 - R_{dc}/R_{ac}} \quad \text{meters} \qquad \text{(B-8)}$$

For $x > 100$, the skin depth δ, for copper is given by

$$\delta = \frac{6.62 \times 10^{-2}}{\sqrt{F}} \quad \text{meters} \qquad \text{(B-9)}$$

and the inside radius of the annular ring is therefore

$$r_\delta = r_c - \delta \quad \text{meters} \qquad \text{(B-10)}$$

The magnetic field intensity of conductor 2 at radius ρ is given by

$$B = \frac{\mu_o I_2}{2\pi\rho} \quad \text{webers/meter}^2 \qquad \text{(B-11)}$$

and encloses that portion of the annular ring of conductor 1 which is shown shaded. To find the area of this shaded segment proceed as follows:

a. Find the area A_1 of the triangle $0_1\ 0_2\ P_c$

$$A_1 = \frac{1}{2} D r_c \sin \alpha_c \quad \text{meters}^2 \qquad \text{(B-12)}$$

b. Find the Area A_2 of sector $O_2 P_c S$

$$A_2 = \frac{1}{2} \rho^2 \beta_c \quad \text{meters}^2 \qquad \text{(B-13)}$$

c. Find the area A_3 of sector $O_1 T_c P_c$

$$A_3 = \frac{1}{2} r_c^2 \alpha_c \quad \text{meters}^2 \qquad \text{(B-14)}$$

d. Obtain the area A_4 bounded by the arcs $P_c S$ and $P_c T_c$, and by the straight line ST_c

$$A_4 = A_3 - (A_1 - A_2)$$

$$A_4 = \frac{1}{2} [r^2 \alpha_c - (D r_c \sin \alpha_c - \rho^2 \beta_c)] \quad \text{meters}^2 \qquad \text{(B-15)}$$

where

$$\alpha_c = \cos^{-1}\left(\frac{D^2 + r_c^2 - \rho^2}{2 D r_c}\right) \qquad \text{(B-16)}$$

$$\beta_c = \cos^{-1}\left(\frac{D^2 + \rho^2 - r^2}{2 D \rho}\right) \qquad \text{(B-17)}$$

e. In similar fashion it will be found that the area A_5 enclosed by the arcs $P_\delta S$ and $P_\delta T_\delta$ and the straight line ST_δ is given by

$$A_5 = \frac{1}{2} [r_\delta^2 \alpha_\delta - (D r_\delta \sin \alpha_\delta - \rho^2 \beta_\delta)] \qquad \text{(B-18)}$$

$$\alpha_\delta = \cos^{-1}\left(\frac{D^2 + r_\delta^2 - \rho^2}{2 D r_\delta}\right) \qquad \text{(B-19)}$$

$$\beta_\delta = \cos^{-1}\left(\frac{D^2 + \rho^2 - r_\delta^2}{2 D \rho}\right) \qquad \text{(B-20)}$$

f. The area A_6 of interest is twice the difference between the areas A_4 and A_5.

$$A_6 = 2(A_4 - A_5) \tag{B-21}$$

With the area determined, the current linked by the flux of conductor 2 can be determined, and the flux linkage computed in the usual manner:

$$d\lambda_{21} = N d\phi_{21} = \left(\frac{J_1 A_6}{I_1}\right) B_2 \, d\rho$$

where

$$J_1 = \frac{I_1}{\pi (r_c^2 - r_\delta^2)}$$

$$d\lambda_{21} = \frac{A_6}{\pi (r_c^2 - r_\delta^2)} \frac{\mu_o I_2}{2\pi\rho} d\rho$$

$$\lambda_{21} = \frac{\mu_o I_2}{2\pi^2 (r_c^2 - r_\delta^2)} \int_{D-r_c}^{D+r_c} \frac{A_6}{\rho} d\rho \tag{B-22}$$

(Note A_6 is included within the integral because of its dependence on ρ).

B.1.7. External mutual linkages. For the same reasons outlined in Section 5 above, the development of external flux linkage relationships cannot be pursued without considering all current carrying paths of the circuit. However, the result may be expressed as a summation of terms of the form

$$\lambda_{ji} = \frac{\mu_o I_j}{2\pi} \ln \frac{1}{D + r_c} \tag{B-23}$$

B.1.8. Conclusions and Results.

The relationships derived in the preceeding section were programed for digital computer calculation. Input data included cable spacing, number of cables of each polarity, their arrangement, and cable diameter. In addition, Table 15-2, reference 12 was read in.

Table B-2 shows the variation of inductance with frequency for one cable type, the largest cable in the distribution system. The maximum error from neglecting the proximity effect is shown to be approximately 3.5% at 10 kc. Since the effect increases with increasing conductor size, this is the worst case.

The values of inductance in Table B-1 were computed using the proximity effect, but in view of the above results, neglegible error would be involved if this effect were ignored.

TABLE B-1

EQUIVALENT DISTRIBUTED

INDUCTANCES AND RESISTANCES

Cable Type:	SSGA 800	SSGA 800	SSGA 650	SSGA 400	SSGA 300	DSGA 125
No. of Pairs:	3	2	3	1	1	1
Frequency	Distributed Inductance,					
0	.39246	.27196	.41250	.19204	.20192	.15358
100 kc	.34301	.23793	.36339	.17392	.18339	.14009
1 Mc	.31875	.22225	.33535	.16800	.17990	.13583
10 Mc	.29277	.20550	.31285	.15885	.16876	.12999
	Distributed Resistance,					
0	.02057	.03086	0.2589	.12360	.17255	.205407
100 kc	.66219	.99328	.74139	2.82058	3.33856	2.5928
1 Mc	2.07430	3.11378	2.32869	8.81258	10.41232	8.0331
10 Mc	6.55855	9.84664	7.3640	27.8678	32.9266	25.4029
$L_{dc}/L_{100\,kc}$	1.14	1.14	1.13	1.10	1.10	1.10

TABLE B-2

The Variation of Distributed Inductance with Frequency

a. Considering skin and proximity effects
b. Considering skin effect alone

(2 pairs of SSGA 800 calbes, separated 1.6 inches)

Frequency cps	Inductance, a Microhenrys/meter	Inductance, b Microhenrys/meter
0	0.27196115	0.27187966
10	.27219310	.27173755
100	.275593862	.26287288
10^3	.25767800	.22602490
10^4	.24721412	.21185031
10^5	.23793139	.20727483
10^6	.22225427	.20587376
10^7	.20550048	.20542194
10^8	.20535731	.20527907

B.2. Distributed Capacitance.

B.2.1. Single Conductor Cable.

Enclosure (5) to reference [2] provides a tabulation of shunt capacitances for SSGA type cables, sizes 3 through 2000. For the multiconductor case, where half the cables carry current in one direction and the other half carry the return current, the total distributed capacitance is the tabulated value multiplied by the number of conductor pairs (parallel addition of the capacitances of like polarity cables) and divided by two (the series addition of capacitance between cables of opposite polarities). An additional factor is included to convert from microfarads-per-thousand-feet to microfarads-per-meter.

2.2 Two Conductor Cable.

The relationship for the capacitance between two conductors enclosed within a conducting sheat is developed by Atwood [1] . After adjusting for units, the equation becomes:

$$C = \frac{27.8\,k}{\ln\left[\frac{2S}{r_c}\cdot\frac{r_o^2-S^2}{r_o^2+S^2}\right]} \quad \left(\frac{pf}{m}\right)$$

k = relative permittivity of the dielectric surrounding the conductors

S = displacement of the center of the conductors from the center of the cable

r_c = radius of the conductor

r_o = radius of the enclosing sheath.

For a dielectric with relative permittivity $k = 5$,

$$C = \frac{139.}{\ln\left[\frac{2S}{r_c}\,\frac{r_o^2-S^2}{r_o^2+S^2}\right]}$$

B.3. Distributed Resistance.

The d-c resistance per unit length was first calculated for a single conductor for each of the cable sizes. This value was then adjusted for the various cable configurations in the same manner as the capacitances: a three pair cable being considered as three parallel sets of two series resistances.

Using the methods of reference [12], these d-c values were adjusted to account for skin effect, and 0.1 mc values were found. The increase was, in general, a resistance 25 to 30 times the d-c value. The results are summarised in Table B-1.

The resistance calculations were done in conjunction with the inductances discussed in section B.1, although the resistance does not include a proximity effect.

B.4. Calculation of Lumped Equivalent Circuit Values.

The preceeding sections of this appendix derive the equivalent inductance, capacitance, and resistance per unit length of the various cable configurations. The definitions in Section 3.2 and Equations (3-30) are the means of computing the equivalent circuits values from them; the line's length is the other factor. For cable number 3, at 0.1 mc,

$$\ell = 67.056 \text{ meters}$$

$$L = 0.363389 \text{ microhenrys/meter}$$

$$C = 0.00256\ 864 \text{ microfarads/meter}$$

$$v = \frac{1}{\sqrt{LC}} = 32.7312 \times 10^6 \text{ M/sec}$$

Table B.4. shows the values used in this model, the characteristic impedances, and the loss parameters (which are subsequently neglected).

$$Z_o = \sqrt{\frac{j\omega L + R}{j\omega C}} \approx \sqrt{\frac{L}{C}}$$

$$\alpha l = \frac{R l}{2 Z_o}$$

CABLE NO.	2	3	4	5	6	7	8	9	10	11
ℓ, m	45.720	67.056	35.052	15.240	16.764	53.340	39.624	54.864	45.720	9.144
L, μhy/m	0.34302	0.36339	0.23793	0.18339	0.14009	0.23793	0.34302	0.23793	0.17392	0.14009
C, pf/m	1,399.06	2,568.64	932.71	335.00	263.48	932.71	1,399.06	932.70	381.70	263.48
v, m/s	45.6483	32.7312	67.1276	124.2436	164.5988	67.1276	45.6483	67.1276	122.7344	164.5988
$\omega\ell/v$, rad	0.62931	1.28723	0.3289	0.07707	0.06399	0.49927	0.59540	0.51353	0.23406	0.03491
" 0-'	36-3.0	73-45.1	18-47.8	4-24.9	3-39.9	28-36.3	31-14.9	29-25.3	13-24.6	2-0.0
L_s, μhy	8.1052	11.3793	4.1518	1.3987	1.0140	6.4795	6.9658	6.7083	3.8406	0.6408
C_p, μf	0.05981	0.09464	0.32114	0.005358	0.004414	0.0477	0.05273	0.04894	0.01728	0.002411
Z_o, Ω	15.6581	11.8942	15.9718	22.8750	23.0586	15.9718	15.6581	15.9718	21.3457	23.0586
R, mil Ω/m	0.66219	0.74139	0.99329	3.33856 34.514	2.59279 33.948	0.99329	0.66219	0.99329	2.82058	2.59279
$\alpha\ell \times 10^3$	0.9668	2.090	1.090	1.112	0.9425	1.658	0.8379	1.706	3.021	0.5032
$\sin\frac{\omega\ell}{v}/\alpha\ell$	608.7	338.4	295.7	69.24	67.85	288.7	619.2	287.9	76.72	69.35

TABLE B-4

Lumped-Equivalent-Circuit Values and Transmission

Line Parameters

APPENDIX C

Passive Circuit Models

C.1. The d-c Motors.

Figure (C-1) is an equivalent circuit of a separately excited d-c motor of the type driving the Trim and Drain Pumps. The known data, from which an entirely electrical circuit is derived, include:

the output power
the line voltage
the motor speed
the resistance and the time constants of the field and armature paths
the moment of inertia.

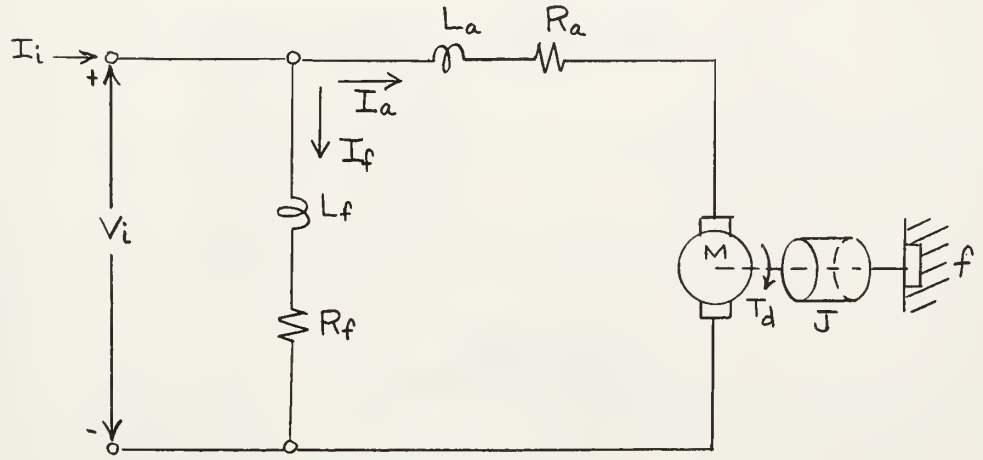

Figure C-1
Equivalent Circuit of Separately Excited d-c Motor

The dynamic behavior of the motor is illustrated by means of a linear signal flow graph, Fig. (C-2).

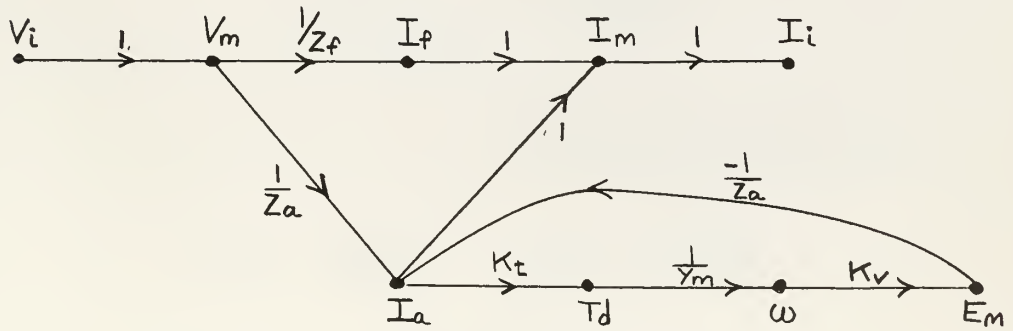

Figure C-2
Flow Graph of Motor's Dynamic Behavior

In the ensuring development, all relations are based upon a consistent system of units: when nameplate data is used to obtain quantitative results, additional conversion constants may be required. The use of constants - in lieu of linear functions of the field current, I_f - as proportionality factors relating armature current, I_a, to developed torque, T_d, and relating motor speed, ω to generated emf, E_m, is justified when the time constant of the motor's field is compared with the period of the expected transients. The relatively large time constant of the field means an almost invariant current during the transient.

Now consider the electrical circuit of Fig. (C-3):

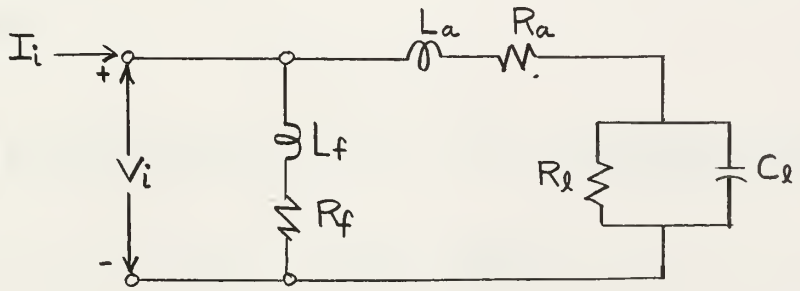

Figure C-3
Equivalent Circuit

The two circuits, the motor and the R-L-C, are similar. Viewed from an external point, they are equivalent (under the assumption of constant field current) if:

$$\frac{1}{Y_l} = \frac{K_t K_v}{Y_m}$$

$$\frac{1}{sC_l + 1/R_l} = \frac{K_t K_v}{sJ+f}$$

$$= \frac{1}{(sJ/K_t K_v) + (f/K_t K_v)}$$

$$C_l = \frac{J}{K_t K_v} \qquad R_l = \frac{K_t K_v}{f}$$

The values of K_t, K_v and f may be derived from the given machine data and from an assumed overall conversion efficiency, η.

$$\eta \triangleq \frac{\text{Power delivered to load}}{\text{Power supplied to input terminals}} = \frac{P_o}{P_i} \qquad \text{(C-1)}$$

Using (C-1) and the assumed efficiency, the power input is found:

$$P_i = P_o/\eta \qquad \text{(C-1a)}$$

Then:
$$I_i = P_i/V_i \qquad \text{(C-2)}$$

and:
$$I_f = V_i/R_f \qquad \text{(C-3)}$$

(At steady state, all the terms with time derivative dependence will go to zero.)

$$I_a = I_i - I_f \qquad \text{(C-4)}$$

The power dissipated as heat in field and armature resistance losses is

$$P_{elec.} = I_f^2 R_f + I_a^2 R_a \qquad \text{(C-5)}$$

The difference between power supplied and electrical losses is the mechanical power developed at the shaft:

$$P_{mech} = P_i - P_{elec.} \qquad \text{(C-6)}$$

But

$$P_{mech} = T_d \cdot \omega \qquad \text{(C-7)}$$

and
$$T_d = K_t \cdot I_a \qquad \text{(C-8)}$$

Eliminating T_d from (C-7) and (C-8) and solving for K_t:

$$K_t = \frac{P_{mech}}{\omega I_a} \qquad \text{(C-9)}$$

The friction coefficient may now be found using the relation

$$T_d = K_t \cdot I_a = \omega f \qquad \text{(C-10)}$$

$$f = K_t \cdot I_a / \omega \qquad \text{(C-10a)}$$

The voltage, E_m, generated by the armature is a function of the coil geometry, the rotor speed, and the magnitude of the stationary magnetic field. The coil geometry is fixed and the stationary magnetic field is constant. Therefore,

$$E_m = K_v \cdot \omega \qquad \text{(C-11)}$$

$$K_v = E_m / \omega \qquad \text{(C-11a)}$$

but $$E_m = V_i - I_a \cdot R_a \qquad \text{(C-12)}$$

therefore $$K_v = (V_i - I_a R_a)/\omega \qquad \text{(C-13)}$$

With the Trim and Drain Pump, the equivalent circuit values are found by

$$P_i = 125/.90 = 139 \text{ HP} = 103.8 \text{ kw}$$

$$I_i = (103.8 \text{ kw})/(.250 \text{ kv}) = 415 \text{ a}$$

$$I_f = 250/61.7 = 4.05 \text{ a}$$

$$\therefore \quad I_a = 415 - 4.05 = 411 \text{ a}$$

$$P_{mech} = 103.8 - \left[(4.05)^2(61.7) + (411)^2(0.0175)\right] \times 10^{-3}$$
$$= 99.9 \text{ kw}$$

$$K_t = \frac{99.9 \times 10^3 \times 60}{2\pi \times 3.5 \times 10^3 \times 4.11 \times 10^2} = 0.664 \ \frac{\text{newt.-m}}{\text{amp}}$$

$$f = \frac{0.664 \times 4.11 \times 60 \times 10^3}{2\pi \times 3.5 \times 10^3} = 0.741 \ \frac{\text{newt-m}}{\frac{\text{rad.}}{\text{sec.}}}$$

$$K_v = \frac{250 - 411 \times 0.0175}{367} = 0.664 \ \frac{\text{volts}}{\frac{\text{rad}}{\text{sec}}}$$

$$R_\ell = \frac{0.664 \times 0.664}{0.741} = 0.594 \ \Omega$$

$$L_f = 0.8 \times 61.7 = 49.4 \text{ hy}$$

$$L_a = 0.0175 \times 0.035 = 0.612 \text{ millihenrys}$$

$$C_\ell = \frac{59 \times 4.214 \times 10^{-2}}{(.664)^2} = 5.65 \text{ f}$$

C.2. The Battery.

The storage battery is extremely nonlinear. Its internal resistance varies with the current, the rate of change of current, and with the degree of charge [17] . It has inductance [15] , and two qualities which resemble capacitance -overvoltage and polarization.

Figure C-4 is the model advocated by reference [15] and [19] for short time studies.

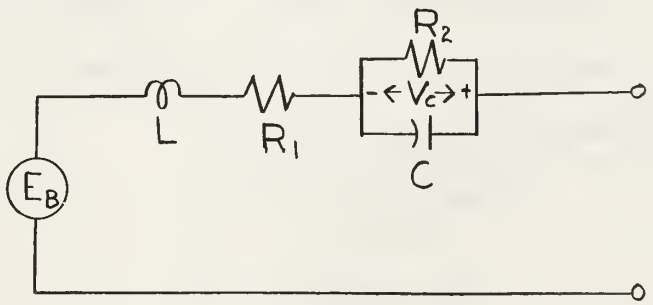

Figure C-4
Equivalent Circuit for Battery

The model is derived in [19] to explain the short time (one second) effects, under relatively low current, seen when the applied voltage is switched. There it is asserted that for a single cell, C will be about 0.016

farads per rated ampere hour and that R_2 will be 0.2 ohms per ampere hour. L is shown to approach 0.15 microhenrys for a single cell of the rating considered in this simulation, although the effects of the inductance are not visible in the reference's results.

Reference [14] discusses the overvoltage that appears while the battery is being charged and is nearly at its rated capacity. The overvoltage's decay is also shown, under open circuit conditions and it appears to have a time constant in the neighborhood of 65 seconds, with the overvoltage starting at 22.5% of the nominal cell voltage. This reference also gives, as experimental data, the value of 40 micro-ohms per cell under short circuit conditions of less than 0.5 seconds duration. Extrapolating the values of R_2 and C from reference 19 to the 6,500 ampere-hour battery gives an overvoltage decay time constant of 135 seconds, which is considered a good comparison to the 65 seconds from reference [14].

The battery in this study will be 126 cells, each of 2.02 volts, in series.

Since this study is concerned with transients, one case should concern the presence of overvoltage. For this, the following values would be used:

E_b: 255 v (nominal battery voltage)
V_c: 62.4 v (initial overvoltage)
L : 975 microhenrys
C : 60 kfarads

R_1: 0.00392 ohms
R_2: 0.00108 ohms

This network and initial voltage match the open circuit overvoltage decay and the steady state internal resistance.

In the initial simulations, the overvoltage is not considered and the battery is considered to be discharging. For this situation, the capacitor is removed from the circuit and the two resistances are combined.

C.3. The Voltage Regulator.

When power is flowing from the a-c side (through a high voltage d-c stage) to the d-c side, the active elements are SCR-1 and Diode D-2 [7] ; no current passes through D-1 or SCR-2. Paths 1 and 2, in Fig. C-5 are alternately followed as SCR-1 is switched to its open or blocking state. Where single elements are shown, there are actually parallel strings of series

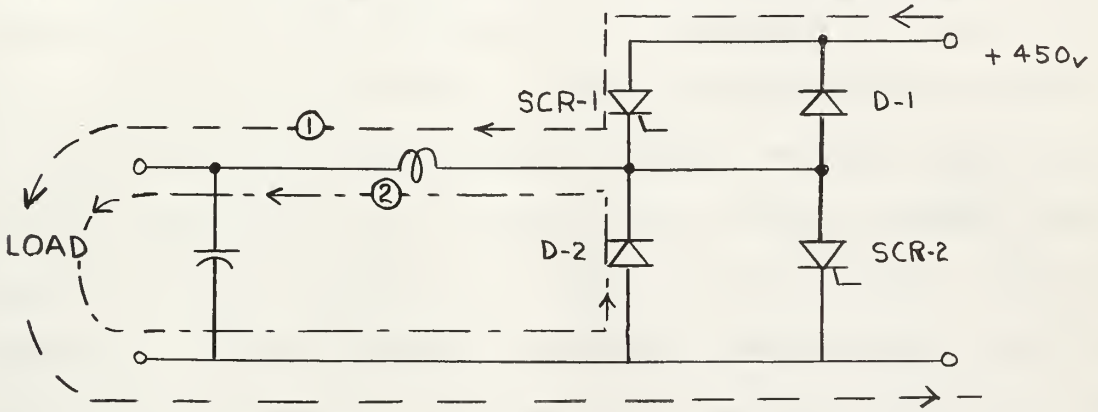

Figure C-5
Current paths, a-c to d-c operation

elements.

Reference [7] gives a value, not otherwise available, from the characteristic curve for a single, open, SCR. This value of E/I (for the combination) is taken as defining a resistance, and this resistance is taken as the linear approximation to the SCR in its conducting state. Figure (C-6)illustrates this approximation.

Figure (C-6)
SCR approximated by a resistance
R = 3.03 milli-ohms

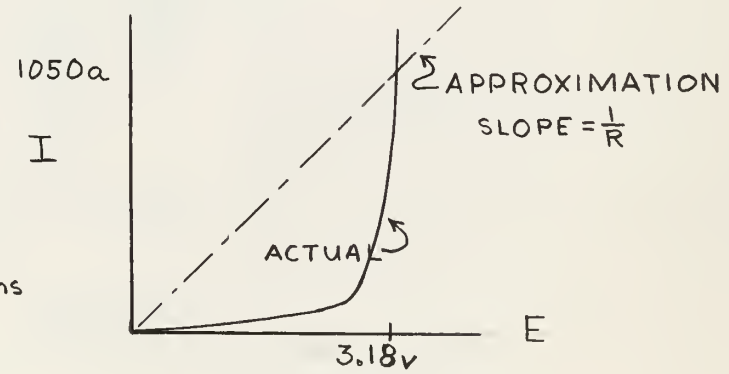

Figure C-6

For the diode, only some power dissipation figures were given. For the first approximation, it is assumed that power is dissipated only during the conduction period, and that the diode current has a square waveform. This leads to a value of 0.796 milliohms for the diode in its conducting state.

When either the diode or the SCR is in its blocking state, it has practically all the 450 volts across it. Without data as to the "reverse characteristics" of such devices, a first approximation is to consider them as perfect switches, with an infinite impedance in their reverse direction. A second approximation is to consider them as passing a leakage current equal to one-ten thousandth of the normal operating current. This order of magnitude is based on that of the small solid state devices. On this basis, the blocking resistance of the Diode and of the SCR is taken to be 4,260 ohms.

The results is that two linear circuits are alternately switched into the network, as shown in Fig. (C-7).

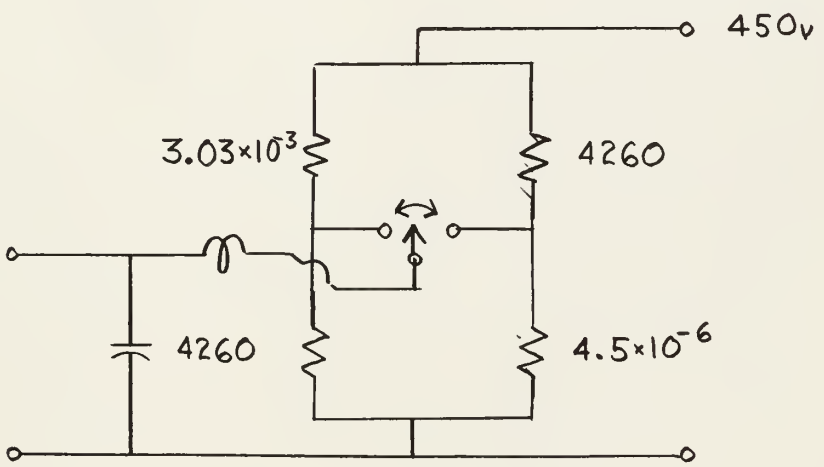

Figure C-7
Equivalent Circuit of d-c Side of Voltage Regulator